Adaptive Time-Step Control for Nonlinear Fluid-Structure Interaction

Lukas Failer[a], Thomas Wick[b,1]

[a] *Chair of Optimal Control, Technische Universität München, Fakultät für Mathematik, Boltzmannstraße 3, 85748 Garching b. München, Germany*
[b] *Centre de Mathématiques Appliquées, École Polytechnique, Université Paris-Saclay, 91128 Palaiseau, France*

Abstract

In this work, we consider time step control for variational-monolithic fluid-structure interaction. The fluid-structure interaction (FSI) system is based on the arbitrary Lagrangian-Eulerian approach and couples the incompressible Navier-Stokes equations with geometrically nonlinear elasticity resulting in a nonlinear PDE system. Based on the monolithic setting, we develop algorithms for temporal adaptivity that are based on a rigorous derivation of dual-weighted sensitivity measures and heuristic truncation-based time step control. The Fractional-Step-theta scheme is the underlying time-stepping method. In order to apply the dual-weighted residual method to our setting, a Galerkin interpretation of the Fractional-Step-theta scheme must be considered. All developments are substantiated with several numerical tests, namely FSI-benchmarks, including appropriate extensions, and a flapping membrane example.

Keywords: nonlinear fluid-structure interaction; arbitrary Lagrangian-Eulerian; time adaptivity; dual-weighted residual method; truncation error; benchmark tests
2000 MSC: 2010 76D05; 74F10; 65M60; 35Q74

1. Introduction

Fluid-structure interaction (FSI) belongs still to the most prominent examples of a nonlinear multiphysics PDE system despite that numerous studies have appeared. In this paper, we focus on a topic that in general has received less attention for FSI: namely temporal discretization schemes and adaptive time step control. The key goals of this work are systematic developments of algorithms for time step control and a detailed computational analysis.

In classical fluid-structure interaction, the isothermal, incompressible Navier-Stokes equations are coupled with nonlinear elasticity. The former system is of parabolic type and describes fluid flow, whereas the latter equation serves for a solid description and is of hyperbolic character. Possible applications range from aeroelasticity, over mechanical engineering, up to computational medicine and medical engineering. For references about these applications, we exemplary refer to the books [14, 28, 30, 13, 5, 57].

Due to the moving domains, an important aspect in FSI is related to the coupling of the fluid with the solid. A prominent coupling technique is the nowadays standard arbitrary Lagrangian-Eulerian (ALE) technique [20, 39, 42, 51, 27, 63, 64], which can be classified as an interface-tracking method. Here, the flow equations are re-written such that their coordinate system matches the Lagrangian framework of the solid. The resulting formulation using variational-monolithic coupling in the reference configuration is outlined in [40, 58, 24].

To date, much effort has been spent on the spatial discretization of fluid-structure interaction and in particular on adaptivity in space (see again [14, 28, 30, 13, 5, 57]). Equally important is the accurate computation of certain quantities of interest (so-called goal functionals). Several studies on goal functional evaluations using the dual-weighted residual (DWR) method [7, 8] can be found in [34, 23, 26, 72, 56, 69].

However, temporal discretization, a flexible choice of time-stepping schemes, and temporal adaptivity are as important as the spatial discretization. Intrinsically, this is clear because the Navier-Stokes equations are of parabolic type and the solid equations are of hyperbolic nature and both ask for different conservation properties that should be reflected in their temporal discretization.

Email addresses: lukas.failer@ma.tum.de (Lukas Failer), thomas.wick@polytechnique.edu (Thomas Wick)

As previously mentioned, we focus on monolithic schemes because of their robustness (e.g., the added-mass effect [15]) and the possibility of employing fully implicit time discretization schemes without numerically-caused restrictions on the time step size. Recent studies and a detailed computational analysis of different time-stepping schemes (using uniform time step sizes) have been undertaken in [67, 59]. Another interesting study has been presented in [48] in which different time discretization schemes for monolithic FSI have been investigated. A temporal two-scale approach of monolithic fluid-structure interaction coupled to chemistry has been proposed in [29]. A study for time step control for a partitioned (simplified) FSI approach, including thermal coupling, has been proposed in [10]. In this last study, adaptivity in time is based on heuristic error estimators. A rigorous derivation of an adaptive scheme using local adjoint sensitivity measures in the frame of FSI is missing in the existing literature.

Using this methodology, namely the previously mentioned DWR method, with application to time step control has been developed for the incompressible Navier-Stokes equations [9] and also the Black-Scholes equation [32]. Very recently, time step control for parabolic problems and the Navier-Stokes equations have been developed in [50, 49]. Moreover, these authors achieved to design a Petrov-Galerkin interpretation of the second-order-in-time, strongly A-stable Fractional-Step-theta scheme [12] on which their adaptive algorithms have been applied to.

Our main contribution in this work is an extension of the lastly mentioned approach to variational-monolithic fluid-structure interaction. We first design the Fractional-Step-theta scheme in terms of a Galerkin scheme and then formulate goal-oriented error estimation. The Galerkin interpretation requires the choice of specially weighted test functions which we explain in detail and that are originally based on the studies presented in [50, 49]. The key challenge is a careful design and interpretation of the adjoint (backward-in-time) time-stepping scheme. Here, we explain all necessary steps and details of the adjoint equations. In order to enhance the quality of these findings, we also develop an heuristic indicator based on measuring the local truncation error. Here, we adopt the idea from [65] and augment the resulting estimator with the help of [35, 44]. Such heuristic approaches for time step control applied to viscous flow (i.e., the Navier-Stokes equations) are studied elsewhere [65, 44, 45, 36].

To justify the superpriority of the Fractional-Step-theta scheme for FSI simulations, we also provide further comparisons (employing uniform time step sizes) to other popular second-order time-stepping schemes such as the A-stable, second-order Crank-Nicolson scheme, the shifted, strictly A-stable, second-order Crank-Nicolson [54, 37] and the Rannacher [47, 53] time-stepping scheme. In the last approach, the basis is the Crank-Nicolson scheme with intermediate backward Euler steps every now and then. The second purpose of this investigation is time grid coarsening. Because both developed error estimators do explicitly allow for larger time steps, it is important to identify schemes that are numerically stable (which is fulfilled since all schemes are implicit) and provide sufficient accuracy in the computation of the numerical solution and the evaluation of goal functionals.

The outline of the paper is as follows: In Section 2 we provide the notation and formulate the monolithic FSI problem in a space-time setting, which enables the use of a Petrov-Galerkin discretization in time and finite elements in space. Next in Section 3 we derive in great detail temporal discretization and finally arrive at the Fractional-Step-theta scheme. We also provide information on spatial discretization and the nonlinear solver in that section. Section 4 represents the key part in which the adaptive scheme using DWR for temporal adaptivity is derived. This is followed by a derivation of an heuristic estimator. Since the solution of the adjoint equation is crucial for the evaluation of the residual based error estimator its presentation has been put into Section 5. Several numerical benchmarks in Section 6 substantiate our algorithmic developments. We recapitulate our findings in Section 7 and provide more details of some equations in the Appendix. The paper is largely based on the PhD thesis of the first author [25], and partly more detailed discussions can be found there.

2. Definitions and Problem Description

2.1. Definitions

The domain $\Omega \subset \mathbb{R}^d$, with dimension $d = 2$, is divided into a fluid domain Ω_f and a solid domain Ω_s such that $\Omega = \Omega_s \cup \Omega_f$. All developments can directly be extended to $d = 3$. The common interface of fluid and solid domain is denoted with $\Gamma_i := \bar{\Omega}_s \cap \bar{\Omega}_f$. The outer boundary is divided into Γ_s, the fixed solid Dirichlet boundary, Γ_f, the outer fluid Dirichlet boundary and the in- and outflow boundaries Γ_{in} and Γ_{out}. All these domains and boundaries are the fixed reference configurations in which the actual computations are undertaken. The physical (moving) domains are indicated by their time dependence '(t)' where necessary.

We introduce in addition the time interval $I := (0, T)$ with end time point T. For several of the presented models in this paper neither existence nor regularity results are available. We will nevertheless state very precise test and solution spaces in such a way that the weak formulations of the models are well defined. For the fluid velocity in the Navier-Stokes equations and the mesh transformation we introduce on the domain Ω_f the spaces

$$V_f := \left\{ \varphi \in H^1(\Omega_f)^d \;\middle|\; \varphi = 0 \text{ on } \Gamma_{in} \cup \Gamma_f \right\}, \quad W_f^v := \left\{ \varphi \;\middle|\; \varphi \in L^2(I; V_f) \text{ and } \partial_t \varphi \in L^2(I; (V_f)^*) \right\},$$
$$W_f^u := \left\{ \varphi \;\middle|\; \varphi \in L^2(I; H_0^1(\Omega_f)) \right\}.$$

And on the solid domain Ω_s we define the corresponding spaces for the displacement and velocity field

$$V_s := \left\{ \varphi \in H^1(\Omega_s)^d \;\middle|\; \varphi = 0 \text{ on } \Gamma_s \right\} \quad \text{and} \quad W_s^u := \left\{ \varphi \;\middle|\; \varphi \in L^2(I; V_s) \text{ and } \partial_t \varphi \in L^2(I; L^2(\Omega_s)^d) \right\},$$
$$W_s^v := \left\{ \varphi \;\middle|\; \varphi \in L^2(I; L^2(\Omega_s)^d) \text{ and } \partial_t \varphi \in L^2(I; (V_s)^*) \right\}$$

with trace zero on parts of the boundary and $(\cdot)^*$ the dual space. As we follow a monolithic approach we have to introduce in addition on the whole domain Ω for the common velocity variable the spaces

$$V^v := \left\{ \varphi \in H^1(\Omega)^d \;\middle|\; \varphi = 0 \text{ on } \Gamma_{in} \cup \Gamma_f \cup \Gamma_s \right\} \quad \text{and} \quad W^v := \left\{ \varphi \;\middle|\; \varphi \in L^2(I; V^v) \text{ and } \partial_t \varphi \in L^2(I; (V^v)^*) \right\},$$

and for the common displacement field and mesh motion variable the spaces

$$V^u := \left\{ \varphi \in H^1(\Omega)^d \;\middle|\; \varphi = 0 \text{ on } \partial\Omega \right\} \quad \text{and} \quad W^u := \left\{ \varphi \;\middle|\; \varphi \in L^2(I; V^u) \text{ and } \partial_t \varphi \in L^2(I; (V^u)^*) \right\}.$$

Finally, for the pressure variable, we introduce the L^2 space $L_f := L^2(\Omega_f)$. To keep the notation as compact as possible here and in what follows, let

$$(u, v) := (u, v)_\Omega, \qquad \langle u, v \rangle_\Gamma := \langle u, v \rangle_\Gamma,$$
$$(u, v)_f := (u, v)_{\Omega_f}, \qquad (u, v)_s := (u, v)_{\Omega_s},$$

be the L^2 inner product on Ω, its sub-domains Ω_f and Ω_s, and on Γ. Furthermore, we use the following notation for inner products on the space-time cylinder:

$$(\!(u, v)\!) = \int_0^T (u, v)\, \mathrm{d}t, \qquad \langle\!\langle u, v \rangle\!\rangle_i = \int_0^T \langle u, v \rangle_\Gamma \, \mathrm{d}t,$$
$$(\!(u, v)\!)_f = \int_0^T (u, v)_f \, \mathrm{d}t, \qquad (\!(u, v)\!)_s = \int_0^T (u, v)_s \, \mathrm{d}t.$$

2.2. A monolithic ALE-formulation for FSI

We regard a configuration where either a fluid flows around an elastic object or flows in an elastic tube. Due to the elastic behavior of the solid, the fluid domain changes over time. In this paper we introduce the arbitrary Lagrangian-Eulerian (ALE) transformation $A : \Omega_f \times I \to \Omega_f(t)$ mapping a reference domain Ω_f on the fluid domain $\Omega_f(t)$. The ALE-mapping can be expressed by $A(x, t) := x + u(x, t)$ using an artificial displacement field u. The gradient of the ALE -mapping will be denoted with $F := Id + \nabla u$ and its determinant with $J := \det(F)$ in the following. The fluid velocity v and pressure p in the following are always defined on the reference domain and fulfill the transformed Navier-Stokes equations. Shear stresses in Newtonian fluids then can be measured using the transformed Cauchy stress tensor

$$\sigma_f = \rho_f^0 \nu_f (\nabla v F^{-1} + F^{-T} \nabla v^T) - p \,\mathrm{Id}$$

with the fluid density ρ_f^0 and the kinematic viscosity ν_f. At the outflow boundary Γ_{out} we enforce a do-nothing outflow condition [38]:

$$\rho_f^0 \nu_f \nabla v F^{-1} - pn = 0$$

with the unit normal vector n.

Problem 1. *(Navier-Stokes equations in ALE coordinates) Let v^D be the extension of the Dirichlet inflow profile on Γ_{in} and $f \in L^2(I; L^2(\Omega)^d)$ be a volume force. We assume the displacements u to be given and smooth. Then, find the velocity $v \in v^D + W_f^v$ and pressure $p \in L^2(I; L_f)$ such that $v(0) = v_0$ and*

$$\begin{aligned} A_F(u, v, p)(\varphi) + A_\Gamma(u, v)(\varphi) &= (\!(\rho_f^0 J f, \varphi)\!)_f && \forall \varphi \in L^2(I; V_f) \\ A_D(u, v)(\xi) &= 0 && \forall \xi \in L^2(I; L_f), \end{aligned}$$

where the transformed momentum equation $A_F(\cdot)(\cdot)$ and the incompressibility constraint $A_D(\cdot)(\cdot)$ are defined by:

$$\begin{aligned} A_F(u, v, p)(\varphi) &:= (\!(J\rho_f^0 \partial_t v, \varphi)\!)_f + (\!(J\rho_f^0 (F^{-1}(v - \partial_t u) \cdot \nabla) v, \varphi)\!)_f + (\!(J\sigma_f F^{-T}, \nabla\varphi)\!)_f \\ A_D(u, v)(\xi) &:= (\!(\operatorname{div}(JF^{-1}v), \xi)\!)_f. \end{aligned}$$

Due to the symmetric stress tensor, the do-nothing outflow condition reduces to

$$A_\Gamma(u, v)(\varphi) := -\langle\!\langle \rho_f^0 \nu_f \nabla v^T F^{-T}, \varphi \rangle\!\rangle_{\Gamma_{out}}.$$

The large deformations of the elastic structure in Ω_s can be described using a nonlinear elastic material law of Saint Venant-Kirchhoff type in several applications. Given the displacement field u, deformations can be characterized in Lagrangian coordinates using the Green-Lagrange strain tensor $E = \frac{1}{2}(F^T F - \mathrm{Id})$, whereby $F = \mathrm{Id} + \nabla u$ is the deformation gradient. The stress in the material then can be given using the second Piola Kirchhoff stress tensor $\Sigma_s = \lambda_s \operatorname{tr}(E)\,\mathrm{Id} + 2\mu_s E$ with the Lamé coefficients λ_s and μ_s. The density of the solid is given by ρ_s^0.

Problem 2. *(Nonlinear elastodynamics equation) Given the volume force $f \in H^1(I; L^2(\Omega_s)^d)$ and the boundary stress $g \in H^1(I; H^{1/2}(\Gamma_i))$ at the interface Γ_i, find the displacement field $u \in W_s^u$ and solid velocity $v \in W_s^v$ such that $u(0) = u_0$, $v(0) = v_0$ and*

$$\begin{aligned} A_S(u, v)(\varphi) &= (\!(\rho_s^0 f, \varphi)\!)_s + \langle\!\langle g, \varphi \rangle\!\rangle_i && \forall \varphi \in L^2(I; V_s), \\ A_V(u, v)(\psi) &= 0 && \forall \psi \in L^2(I; V_s), \end{aligned}$$

whereby

$$\begin{aligned} A_S(u, v)(\varphi) &:= (\!(\rho_s^0 \partial_t v, \varphi)\!)_s + (\!(F\Sigma_s, \nabla\varphi)\!)_s, \\ A_V(u, v)(\psi) &:= (\!(u_t - v, \psi)\!)_s. \end{aligned}$$

Remark 1. *As formulated in the above problem, we demand more regularity for the boundary condition and right-hand side to be on the save side. Then the trace of v at the interface Γ_i is given in the trace sense of H^1 function spaces. Higher regularity of v was explicitely required for well-posedness of fluid-structure interaction as discussed in [17, 18].*

Given the solid displacement field u on Γ_i we can define an extension operator mapping the reference domain Ω_f on the moving fluid domain with

$$u|_{\Omega_s} = u|_{\Omega_f} \text{ on } \Gamma_i \qquad \text{(geometric coupling condition)}.$$

The so called mesh motion can for example be calculated by solving a nonlinear elasticity equation with a pseudo elastic material law. Given the Lamé coefficients

$$\lambda_m := \frac{E_m}{2J(1 + \nu_m)}, \quad \mu_m := \frac{E_m \nu_m}{J(1 + \nu_m)(1 - \nu_m)},$$

where $E_m > 0$ and $\nu_m \in [-1, 0.5]$ (e.g. $\nu_m = -0.1$ works well in practice for the FSI benchmarks) and the linear strain tensor $\varepsilon_m := \frac{1}{2}(\nabla u + \nabla u^T)$, then the Cauchy stress tensor is defined by

$$\sigma_m := \lambda_m \operatorname{tr}(\varepsilon_m)\,\mathrm{Id} + 2\mu_m \varepsilon_m.$$

In Section 6.5, we use a special construction since the two elastic flaps are very thin and mesh distortion will likely occur. For this reason we also carried out tests with a biharmonic mesh motion model as formulated for FSI in [68].

Problem 3. *(Mesh motion equation) Let u^D be the extension of the solid displacement on the interface, then find $u \in u^D + W_f^u$ such that*

$$A_M(u)(\psi) := 0 \quad \forall \psi \in L^2(I, H_0^1(\Omega_f)^d),$$

whereby the semi-linear form $A_M(\cdot)(\cdot)$ is defined by

$$A_M(u)(\psi) := (\!(\sigma_m, \nabla\psi)\!)_f.$$

Solid and fluid equations are coupled by common boundary conditions at Γ_i. We assume a no-slip condition for the fluid. Therefore, the solid and fluid velocities have to coincide at the interface Γ_i, such that

$$v|_{\Omega_s} = v|_{\Omega_f} \text{ on } \Gamma_i \qquad \text{(kinematic coupling condition).}$$

In addition we assume that normal stresses are equal. As we have transformed the fluid equation on the reference domain, fluid and solid stresses are given in the same coordinate system and we demand

$$F_s\Sigma_s n = J\sigma_f F^{-T} n \text{ on } \Gamma_i \qquad \text{(dynamic coupling condition).}$$

Monolithic formulations are well known for nonlinear FSI problems and they are used for example in [40, 58, 24, 68] to obtain robust numerical algorithms keeping errors occurring from the coupling conditions small. Therein the kinematic coupling condition is enforced by choosing a smooth trial space for the common velocity variable defined on the whole domain. Furthermore, due to a test function defined in the same velocity space V^v, the dynamic coupling condition is automatically fulfilled. In the case of the here considered nonlinear FSI problem this leads to

Problem 4. *(Fluid-structure interaction problem) Find a velocity $v \in v^D + W^v$, a displacement $u \in W^u$ and a pressure $p \in L^2(I; L_f)$ fulfilling the weak formulation:*

$$\begin{aligned}
(\!(J\rho_f^0 \partial_t v, \varphi)\!)_f + (\!(J\rho_f^0 (F^{-1}(v - \partial_t u)\cdot\nabla)v, \varphi)\!)_f + (\!(J\sigma_f F^{-T}, \nabla\varphi)\!)_f & \\
+ (\!(\rho_s^0 \partial_t v, \varphi)\!)_s + (\!(F\Sigma_s, \nabla\varphi)\!)_s & \\
- \langle\!\langle \rho_f^0 \nu_f F^{-T}\nabla v^T, \varphi \rangle\!\rangle_{\Gamma_{out}} - (\!(J\rho_f^0 f, \varphi)\!)_f - (\!(\rho_s^0 f, \varphi)\!)_s = 0 & \qquad \forall \varphi \in L^2(I; V^v), \\
(\!(\sigma_m, \nabla\psi)\!)_f + (\!(\partial_t u - v, \psi)\!)_s = 0 & \qquad \forall \psi \in L^2(I; V^u), \\
(\!(\mathrm{div}(JF^{-1}v), \xi)\!)_f = 0 & \qquad \forall \xi \in L^2(I; L_f),
\end{aligned}$$

with the initial conditions $v(0) = v^0$ and $u(0) = u^0$.

To write the FSI problem in a more compact form, we introduce for the volume force the semilinear form

$$F(u)(\varphi) := (\!(J\rho_f^0 f, \varphi)\!)_f + (\!(\rho_s^0 f, \varphi)\!)_s$$

and for the initial conditions the semilinear forms

$$I_V(v)(\varphi) := (v_0 - v(0), \varphi(0)), \quad I_U(u)(\psi) := (u_0 - u(0), \psi(0)).$$

If we define in addition the solution space X and the combined test space $\tilde{X}$, with

$$X := W^v \times W^u \times L^2(I; L_f), \quad \text{and} \quad \tilde{X} := L^2(I; V^v) \times L^2(I; V^u) \times L^2(I; L_f),$$

we can write in the sequel the continuous fluid-structure interaction problem in a very compressed form by

Problem 5. *Find $U := (v, u, p) \in U^D + X$ such that*

$$A(U)(\Phi) = 0 \quad \forall \Phi \in \tilde{X} \tag{1}$$

with $\Phi := (\varphi, \psi, \xi) \in \tilde{X}$ and the semi-linear form $A(\cdot)(\cdot)$ is defined by

$$\begin{aligned}
A(U)(\Phi) :=& A_F(U)(\varphi) + A_S(U)(\varphi) + A_\Gamma(U)(\varphi) - F(U)(\varphi) - I_V(v)(\varphi) \\
&+ A_V(U)(\psi) + A_M(U)(\psi) - I_U(u)(\psi) + A_D(U)(\xi)
\end{aligned}$$

We will assume in the following that there exists a unique smooth solution for Problem 5. For more information on the assumptions on initial data and regularity of the domain to guarantee existence and uniqueness for FSI we refer for example to [43, 33, 17, 18]. Thereby, we would like to emphasize that existence results for more general domains, as regarded in the numerical calculations later, only have been proven for the linear FSI problem as for example in [21, 22, 1, 2], yet.

3. Discretization in Time and Space

In this section, we first introduce temporal discretization in great detail and derive an arbitrary theta scheme for fluid-structure interaction. Later we briefly comment on the spatial discretization based on finite elements. The resulting nonlinear discrete problems are solved with a Newton solver. We apply in the first Section 3.1 the Petrov-Galerkin discretization suggested by Meidner and Richter in [49] and [50]. The goal is a systematic derivation of a Fractional-Step-theta time-stepping scheme for the fluid-structure interaction Problem 5. A more detailed derivation can be found in [25].

3.1. Time discretization

In the following we partition the time interval $I = (0, T)$ in M subintervals $I_m = (t_m, t_{m-1})$ with $t_0 < t_1 < ... < t_M = T$. On every time interval I_m we define a parameter $\theta_m \in [0, 1]$ and the interval length $k_m := t_m - t_{m-1}$.We are going to discretize the velocity and displacement field using the piece-wise linear subspaces $W_k^v \subset W^v$ and $W_k^u \subset W^v$ with

$$W_k^v = \left\{ v_k \in C(\bar{I}, V^v) \;\middle|\; v_k|_{I_m} \in P_1(I_m, V^v), m = 1, 2, ..., M \right\},$$
$$W_k^u = \left\{ u_k \in C(\bar{I}, V^u) \;\middle|\; u_k|_{I_m} \in P_1(I_m, V^u), m = 1, 2, ..., M \right\}.$$

To take the pressure fully implicit we use here the piece-wise constant and discontinuous test space $W_k^p \subset L^2(I; L_f)$ with

$$W_k^p = \left\{ p_k \in L^2(I, L_f) \;\middle|\; p_k|_{I_m} \in P_0(I_m, L_f), m = 1, 2, ..., M \right\}.$$

For the incompressibility constraint we use the same space W_k^p as test function. Thereby, the semidiscrete pressure can be interpreted as Lagrange multiplier of the divergence condition in each time interval I_m, later. To result in a Fractional-Step-theta time stepping scheme, we choose for the momentum equation and the extension a discontinuous test space

$$W_{k,\theta}^v = \left\{ \varphi_k \in L^2(I, V^v) \;\middle|\; \varphi_k|_{I_m} \in P_0^\theta(I_m, V^v), m = 1, 2, ..., M \text{ and } \varphi(0) \in V^v \right\},$$
$$W_{k,\theta}^u = \left\{ \varphi_k \in L^2(I, V^u) \;\middle|\; \varphi_k|_{I_m} \in P_0^\theta(I_m, V^u), m = 1, 2, ..., M \text{ and } \varphi(0) \in V^u \right\},$$

whereby the slope on each time interval I_m depends on the parameter θ as we choose

$$P_0^\theta(I_m, V^v) := \{\omega_{m,\theta}\bar{\varphi}_{k,m} | \bar{\varphi}_{k,m} \in V^v\} \quad \text{and} \quad P_0^\theta(I_m, V^u) := \{\omega_{m,\theta}\bar{\varphi}_{k,m} | \bar{\varphi}_{k,m} \in V^u\},$$

with

$$\omega_{m,\theta}(t) = 1 + 6\Big(\theta_m - \frac{1}{2}\Big)\frac{2t - t_{m-1} - t_m}{k_m}.$$

Therefore, if we look for the semidiscrete solution $U_k := (v_k, u_k, p_k) \in X_k := W_k^v \times W_k^u \times W_k^p$ and if we replace the test space $\tilde{X}$ in Problem 5 with the just defined semidiscrete space $X_{k,\theta} := W_{k,\theta}^v \times W_{k,\theta}^u \times W_k^p$ we automatically obtain the Petrov Galerkin semi-discretization of the state equation:

Problem 6. *Find $U_k \in U^D + X_k$ such that*

$$\begin{aligned} A_F(U_k)(\varphi_k) + A_S(U_k)(\varphi_k) + A_\Gamma(U_k)(\varphi_k) &= F(U_k)(\varphi_k) + I_V(U_k)(\varphi_k) && \forall \varphi_k \in W_{k,\theta}^v, \\ A_M(U_k)(\psi_k) + A_V(U_k)(\psi_k) &= I_U(U_k)(\psi_k) && \forall \psi_k \in W_{k,\theta}^u, \\ A_D(U_k)(\xi_k) &= 0 && \forall \xi_k \in W_k^p. \end{aligned}$$

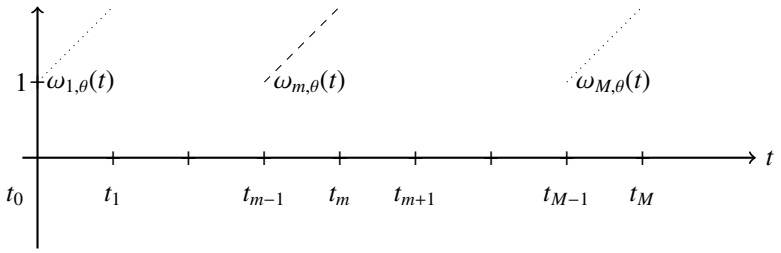

Figure 1: Plot of the basis functions $\omega_{m,\theta}$.

Now we exploit the fact, that every function $(\varphi_k, \psi_k, \xi_k) \in W^v_{k,\theta} \times W^u_{k,\theta} \times W^p_k$ can be represented as linear combination of the basis functions $\omega_{m,\theta}$ presented in Figure 1 and the characteristic function $\mathcal{X}_{I_m}$ such that

$$\varphi_k = \sum_{m=0}^{N} \varphi_m \omega_{m,\theta}(t), \quad \psi_k = \sum_{m=0}^{N} \psi_m \omega_{m,\theta}(t) \quad \text{and} \quad \xi_k = \sum_{m=1}^{N} \mathcal{X}_{I_m}(t) \xi_m,$$

with $(\varphi_m, \psi_m, \xi_m) \in V^v \times V^u \times L_f$. As $(v_k, u_k) \in W^v_k \times W^u_k$ are piecewise linear functions in time, we can use the representation

$$v_k = \sum_{i=0}^{M} v_{k,m} \omega_m(t) \quad \text{and} \quad u_k = \sum_{i=0}^{M} u_{k,m} \omega_m(t)$$

with $v_{k,m} := v_k(t_m)$ and $u_{k,m} := u_k(t_m)$ whereby $\omega_m(t)$ is a standard hat function on the time grid as displayed in Figure 2.

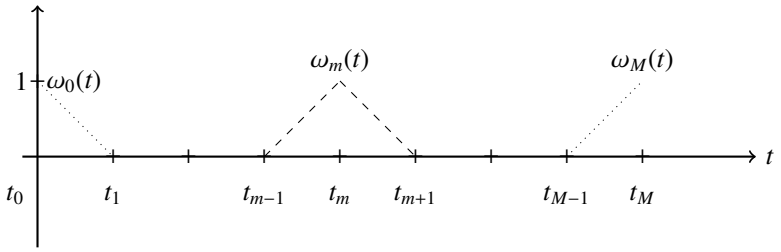

Figure 2: Plot of the basis functions ω_m.

In addition we can use for the semi-discretized pressure the representation

$$p_k = \sum_{m=1}^{M} p_{k,m} \mathcal{X}_{I_m}(t) \quad \text{with} \quad p_{k,m} := \frac{1}{k_m} \int_{I_m} p_k \mathrm{d}t.$$

Due to the nonlinearity of the problem, we have to evaluate the time-integrals with an appropriate quadrature rule. Instead of using a quadrature rule of high order, we are going to evaluate the inner product in time using the following theta-dependent trapezoidal rule

$$\int_{I_m} h(t) \omega_{\theta,m}(t) \, \mathrm{d}x \approx k_m \{\theta_m h(t_m^-) + (1 - \theta_m) h(t_{m-1}^+)\} \tag{2}$$

suggested in [49] with

$$h(t_m^+) := \lim_{\delta t \to 0^+} h(t_m + \delta t) \text{ and } \quad h(t_m^-) := \lim_{\delta t \to 0^-} h(t_m + \delta t).$$

Thereby, the resulting time-stepping scheme coincides with a standard theta time-stepping scheme and inherits its well known properties. For smooth functions multiplied with the theta-dependent function $\omega_{\theta,m}$, the quadrature rule is of second order convergence, see [49].

As the test functions in the incompressibility condition are theta independent, we use a trapezoidal rule here. If we apply the stated quadrature rules and take into account that we have for the derivative in time of $(v_k, u_k) \in W_k^v \times W_k^u$ on every time interval

$$\partial_t v_k\big|_{I_m} = \frac{1}{k_m}(v_{k,m} - v_{k,m-1}) \quad \text{and} \quad \partial_t u_k\big|_{I_m} = \frac{1}{k_m}(u_{k,m} - u_{k,m-1}).$$

It then holds

Problem 7. *Find $U_k \in U^D + X_k$ such that*

$$\tilde{A}(U_k)(\Phi_k) = 0 \quad \forall \Phi_k \in X_{k,\theta}, \tag{3}$$

with

$$\begin{aligned}\tilde{A}(U_k)(\Phi_k) = \sum_{m=1}^{M} \Big[&\tilde{A}_F(U_{k,m}, U_{k,m-1})(\varphi_m) + \tilde{A}_S(U_{k,m}, U_{k,m-1})(\varphi_m) + \tilde{A}_\Gamma(U_{k,m}, U_{k,m-1})(\varphi_m) \\ &+\tilde{A}_M(U_{k,m}, U_{k,m-1})(\psi_m) + \tilde{A}_V(U_{k,m}, U_{k,m-1})(\psi_m) + \tilde{A}_D(U_{k,m}, U_{k,m-1})(\xi_m) \\ &-\tilde{F}(U_{k,m}, U_{k,m-1})(\varphi_m)\Big] - \tilde{I}_V(U_{k,0})(\varphi_0) - \tilde{I}_U(U_{k,0})(\psi_0).\end{aligned}$$

The semi-linear forms $\tilde{A}_F(\cdot,\cdot)(\cdot)$, $\tilde{A}_S(\cdot,\cdot)(\cdot)$, $\tilde{A}_\Gamma(\cdot,\cdot)(\cdot)$, $\tilde{A}_M(\cdot,\cdot)(\cdot)$, $\tilde{A}_V(\cdot,\cdot)(\cdot)$, $\tilde{A}_D(\cdot,\cdot)(\cdot)$ and $\tilde{F}(\cdot,\cdot)(\cdot)$ are summarized in the appendix as well as the initial conditions given by $\tilde{I}_V(\cdot)(\cdot)$ and $\tilde{I}_U(\cdot)(\cdot)$.

Due to linearity of the semilinear form $\tilde{A}(U_k)(\Phi_k)$ with respect to the test functions Φ_k we can rewrite the semi-discretized nonlinear fluid-structure interaction problem as time-stepping scheme.

Problem 8. *Let $(\theta_m)_{m=1}^M \in [0,1]^M$ and $(v_{k,0}, u_{k,0}) = (v_0, u_0)$. Find $(U_{k,m})_{m=1}^M \in (V^v)^M \times (V^u)^M \times L_f^M$ by iterating for $m = 1, ..., M$:*

$$\begin{aligned}\tilde{A}_F(U_{k,m}, U_{k,m-1})(\varphi) + \tilde{A}_S(U_{k,m}, U_{k,m-1})(\varphi) + \tilde{A}_\Gamma(U_{k,m}, U_{k,m-1})(\varphi) = \tilde{F}(U_{k,m}, U_{k,m-1})(\varphi) \qquad &\forall \varphi \in V^v, \\ \tilde{A}_M(U_{k,m}, U_{k,m-1})(\psi) + \tilde{A}_V(U_{k,m}, U_{k,m-1})(\psi) = 0 \qquad &\forall \psi \in V^u, \\ \tilde{A}_D(U_{k,m}, U_{k,m-1})(\xi) = 0 \qquad &\forall \xi \in L_f.\end{aligned}$$

In short notation, similar to Problem 7, we write: Find $(U_{k,m})_{m=1}^M \in (V^v)^M \times (V^u)^M \times L_f^M$ such that

$$\tilde{A}(U_{k,m}, U_{k,m-1})(\Phi_k) = 0 \quad \forall \{\varphi, \psi, \xi\} \in (V^v)^M \times (V^u)^M \times L_f^M. \tag{4}$$

3.2. On the divergence condition

The divergence condition in Problem 8 is only fulfilled in an average sense in every time interval I_m as we demand in the time-stepping scheme at every step $m = 1, ..., M$

$$\frac{k_m}{2}\Big[(\mathrm{div}(J_m F_m^{-1} v_m), \xi)_f + (\mathrm{div}(J_{m-1} F_{m-1}^{-1} v_{m-1}), \xi)_f\Big] = 0 \quad \forall \xi \in L_f.$$

Thereby, errors in the divergence condition are conserved and can accumulate over time. Thus we are going to enforce the divergence condition to be fulfilled in every time point, by using

$$\tilde{A}_D(U_{k,m}, U_{k,m-1})(\xi) = k_m(\mathrm{div}(J_m F_m^{-1} v_m), \xi)_f.$$

If the initial condition is divergence free, both formulations are equivalent. A detailed discussion of this step can be found for the Navier-Stokes equations in [50].

3.3. Theta schemes

The presented Petrov-Galerkin method allows to systematically derive arbitrary theta time-stepping schemes for complex multiphysics problems as the here regarded fluid-structure interaction problem. If we choose $\theta_m = 1$ in every time interval $m = 1, ..., M$, then the resulting time stepping scheme corresponds to an implicit backward Euler method. And we obtain for $\theta_m = 0.5$ a Crank-Nicolson method and for $\theta_m = 0.5 + k_s$, where $k_s \sim k_m$, a shifted Crank-Nicolson time stepping scheme. Furthermore the method includes the Rannacher time-stepping scheme, a Crank-Nicolson time-stepping scheme with Euler stabilization steps in between as presented in [37]. To derive a Fractional-Step-theta scheme, we will always combine three steps to one macro time step with step size k_n and $n = 1, .., M/3$. For $m = 3 \cdot n$, it holds:

$$(k_m, k_{m+1}, k_{m+2}) := (\alpha k_n, (1-\alpha)k_n, \alpha k_n)$$
$$(\theta_m, \theta_{m+1}, \theta_{m+2}) := (\theta, (1-\theta), \theta).$$

If we choose

$$\theta = \frac{1-2\alpha}{1-\alpha} \text{ and } \alpha := 1 - \sqrt{\frac{1}{2}},$$

the resulting Fractional-Step-theta time stepping scheme is known to be A-stable and of second order accuracy [12]. Due to its little numerical dissipation it is in particular well suited when wave equation-type problems (the solid equation) are coupled to parabolic-type problems (i.e., Navier-Stokes for laminar flow) as considered in this paper. In addition, the resulting Fractional-Step-theta time-stepping scheme in Problem 8 coincides with the time discrete Petrov-Galerkin formulation of Problem 6 up to numerical quadrature for the given choice of parameters. We finally recall that the computational cost of the Fractional-Step-theta scheme and the Crank-Nicolson-type approach are of the same order since three-times larger time steps can be employed for the Fractional-Step-theta method.

3.4. Spatial discretization

The time discretized formulation in Problem 8 is the starting point for a conforming Galerkin discretization in space. To this end, we construct finite dimensional subspaces $(V_h^v)^M \times (V_h^u)^M \times L_{f,h}^M \subset (V^v)^M \times (V^u)^M \times L_f^M$ to find an approximate solution to the continuous problem. We use two dimensional shape-regular meshes. A mesh consists of quadrilateral cells K. They perform a non-overlapping cover of the computational domain $\Omega \subset \mathbb{R}^d$. The corresponding mesh is given by $\mathcal{T}_h = \{K\}$. The discretization parameter in the reference configuration is denoted by h and is a cell-wise constant that is given by the diameter h_K of the cell K.

The specific choice of finite elements is the same, namely Q_2^c elements for the displacements. For the precise definition of Q_p^c, where p is the bi-polynomial degree, we refer the reader to [11, 16]. For the flow part we work with two different discretizations. In our first formulation using RoDoBo [60], we work with equal-order Q_1^c/Q_1^c finite elements with LPS-stabilization [6] for discretizing the Navier-Stokes equations. In deal.II [3] (using the FSI-template [70]), we prefer the biquadratic, discontinuous-linear Q_2^c/P_1^{dc} element, which preserves local mass conservation and satisfies the *inf-sup stability*.

The temporally and spatially discretized formulation then reads:

Problem 9. *Let* $(\theta_m)_{m=1}^M \in [0,1]^M$ *and* $(v_{k,0}^h, u_{k,0}^h) = (v_0^h, u_0^h)$. *Find* $(U_{k,m}^h)_{m=1}^M \in (V_h^v)^M \times (V_h^u)^M \times L_{f,h}^M$ *by iterating for* $m = 1, ..., M$:

$$\begin{aligned}
&\tilde{A}_F(U_{k,m}^h, U_{k,m-1}^h)(\varphi^h) + \tilde{A}_S(U_{k,m}^h, U_{k,m-1}^h)(\varphi^h) \\
&\quad + \tilde{A}_\Gamma(U_{k,m}^h, U_{k,m-1}^h)(\varphi^h) - \tilde{F}(U_{k,m}^h, U_{k,m-1}^h)(\varphi^h) = 0 && \forall \varphi^h \in V_h^v, \\
&\tilde{A}_M(U_{k,m}^h, U_{k,m-1}^h)(\psi^h) + \tilde{A}_V(U_{k,m}^h, U_{k,m-1}^h)(\psi^h) = 0 && \forall \psi^h \in V_h^u, \\
&\tilde{A}_D(U_{k,m}^h, U_{k,m-1}^h)(\xi^h) = 0 && \forall \xi^h \in L_{f,h}.
\end{aligned}$$

In short notation, similar to Problem 7, we write: Find $(U_{k,m}^h)_{m=1}^M \in (V^v)_h^M \times (V^u)_h^M \times L_{f,h}^M$ *such that*

$$\tilde{A}(U_{k,m}^h, U_{k,m-1}^h)(\Phi_k^h) = 0 \quad \forall \{\varphi^h, \psi^h, \xi^h\} \in (V^v)_h^M \times (V^u)_h^M \times L_{f,h}^M. \tag{5}$$

3.5. Nonlinear and linear solvers

For solving the nonlinear problem, we employ a Newton solver with backtracking line search and intermediate quasi-Newton steps. The linear subproblems are solved with LU decomposition (a direct solver) and specifically UMFPACK [19].

In more detail at each discrete time step in Problem 9 we solve a nonlinear quasi-stationary problem to find a solution $U^h_{k,m}$ such that

$$\tilde{A}(U^h_{k,m}, U^h_{k,m-1})(\Phi^h_k) = 0 \quad \forall \Phi^h_k \in X^h_k.$$

The Newton algorithm in defect correction notation is summarized in Algorithm 1.

Algorithm 1: Newton Algorithm

For fixed m and h, let an initial Newton guess $U^{h,0}_{k,m}$ be given. Set $j = 0$
while Newton Residual > tol **do**
Compute the update $\delta U^{h,j}_{k,m}$ of the linear defect-correction problem

$$\begin{aligned} \tilde{A}'(U^{h,j}_{k,m}, U^h_{k,m-1})(\delta U^{h,j}_{k,m}, \Phi) &= -\tilde{A}(U^{h,j}_{k,m}, U^h_{k,m-1})(\Phi), \\ U^{h,j+1}_{k,m} &= U^{h,j}_{k,m} + \omega \delta U^{h,j}_{k,m}. \end{aligned} \tag{6}$$

Set $j = j + 1$
end while

Remark 2. *In Algorithm 1 the variable $\omega \in (0, 1]$ is a damping parameter, which is determined by backtracking line search, namely when*

$$\|\tilde{A}(U^{h,j+1}_{k,m})(\Phi_h)\|_{l^2} < \|\tilde{A}(U^{h,j}_{k,m})(\Phi_h)\|_{l^2}.$$

Furthermore, $\tilde{A}'(U^{h,j}_{k,m})(\delta U^{h,j}_{k,m}, \Phi)$ denotes the directional derivative, which is computed as Gateaux derivative. If the Newton matrix is good enough, we do not build it again for the next iteration to reduce the computational cost. The linearization of the semi-linear form $A(\cdot)(\cdot)$ with respect to the primal variable is presented in the appendix. The Gateaux derivative in every time step of the fully discretized semi-linear form $\tilde{A}(\cdot)(\cdot)$ can be formally derived in a similar manner. Details are provided in [25] and [67].

4. Goal-Oriented Error Estimation

4.1. Dual-weighted residual error estimator

To compute the error in a functional of interest, we are going to apply an a posteriori error estimator presented in [49] and [50], which is based on the dual weighted residual (DWR) method developed by Becker and Rannacher [7, 8]. The differentiable functional of interest $\mathcal{J} : X \to \mathbb{R}$ is given by

$$\mathcal{J}(U) = \int_I j_1(U(t)) \, \mathrm{d}t + j_2(U(T)),$$

where $j_1 : X \to \mathbb{R}$ is distributed in time and $j_2 : V^v \times V^u \times L_f \to \mathbb{R}$ measures a value of interest at the final time T.

The error estimator thereby consists of a first part for the discretization error, using the DWR method, and a second part for the numerical quadrature error. The estimation of the quadrature error is necessary due to the discrepancy between the time stepping scheme in Problem 8 and the Petrov-Galerkin formulation in Problem 6. The quadrature error can not be neglected as the applied quadrature rule is only of second order accuracy and therefore of the same order as the approximation error.

For the Fractional-Step-theta time stepping scheme, we only have second order convergence in the macro time steps. The intermediate steps of the Fractional-Step-theta method are not necessarily good approximations to the solution. Hence these steps are omitted in the functional evaluation. Therefore, we introduce the piecewise linear

interpolation $i_{3k} : X_k \to X_k^{\text{macro}}$, such that $i_{3k}U_k$ and U_k coincide on the macro time points t_{3n}. The space X_k^{macro} is defined on the macro time grid

$$t_0 < t_3 < ... < t_{3n} < .. < t_M.$$

To evaluate the error between the functional evaluated using the continuous solution $U \in X$ and the semidiscrete solution on the macro time steps $i_{3k}U_k$, we introduce the Lagrange functional $L : X \times \tilde{X} \to \mathbb{R}$ and the discrete Lagrange functional $\tilde{L} : X_k \times X_{k,\theta} \to \mathbb{R}$ with

$$L(U)(Z) = \mathcal{J}(U) - A(U)(Z), \tag{7}$$

$$\tilde{L}(U_k)(Z_k) = \tilde{\mathcal{J}}(U_k) - \tilde{A}(U_k)(Z_k), \tag{8}$$

whereby we choose $Z \in \tilde{X}$ and $Z_k \in X_{k,\theta}$ to fulfill the first-order necessary condition with respect to the state variable U:

$$A'(U)(\Phi, Z) = \mathcal{J}'(U)(\Phi) \quad \forall \Phi \in X, \tag{9}$$

$$\tilde{A}'(U_k)(\Phi_k, Z_k) = \tilde{\mathcal{J}}'(U_k)(\Phi_k) \quad \forall \Phi_k \in X_k, \tag{10}$$

and $\tilde{\mathcal{J}}(U)$ is the evaluation of $\mathcal{J}(U)$ using the quadrature rule (2). The semidiscrete adjoint equation (10) can be obtained by replacing again the space X in (9) by the semidiscrete space X_k and then apply again the quadrature rule (2). For more details, we refer the reader to Section 5. Then the error between the solution U of Problem 5 and the semidiscrete solution $i_{3k}U_k$ of Problem 8 can be written as

$$\mathcal{J}(U) - \mathcal{J}(i_{3k}U_k) = [\tilde{\mathcal{J}}(U_k) - \mathcal{J}(i_{3k}U_k)] + [L(U)(Z) - \tilde{L}(U_k)(Z_k)].$$

Then using Theorem 1 in [50] we immediately obtain formally:

Theorem 1. *Let $U \in X$ be the solution to Problem 5, $U_k \in X_k$ be the solution to Problem 8 and $Z \in X$ as well as $Z_k \in X_{k,\theta}$ be the adjoint solutions given by* (9) *and* (10)*. Furthermore we denote by $i_{3k}U_k$ the solution on the macro time steps. For the functional error due to time discretization it holds*

$$\mathcal{J}(U) - \mathcal{J}(i_{3k}U_k) = [\mathcal{J}(U_k) - \mathcal{J}(i_{3k}U_k)] + \rho(U_k)(Z_k) + \frac{1}{2}[\rho(U_k)(Z - \pi Z) + \rho^*(Z_k)(U - i_k u)] + R_k \tag{11}$$

with the primal and dual residuals

$$\rho(U)(\Phi) := F(\Phi) - A(U)(\Phi), \quad \rho^*(U, Z)(\Phi) := \mathcal{J}'(U)(\Phi) - A'(U)(\Psi, Z)$$

and a remainder R_k. Here i_k is the nodal interpolation and π the L^2 projection into the discrete spaces $X_{k,\theta}$.

Remark 3. *Third order convergence of the remainder term R_k has been proven in [49] for semilinear parabolic PDEs and in [50] for the Navier-Stokes equations. Due to the lack of regularity in the solid equation and the additional nonlinearity due to the moving domains, the here regarded FSI problem does not fall into the setting considered in the cited papers. Consequently, the proof is much more involved and out of scope in this paper. We can however still show the effectivity of the estimator as a computational method.*

Motivated by super convergence results, as in [62], we use as approximation of the weights a higher order reconstruction as approximation of U and Z. As the intermediate steps of the Fractional-Step-theta time-stepping scheme are not necessarily good approximations, we use the piecewise quadratic reconstruction of the solution on the macro steps suggested in [49, 50]. Using the approximation of the weights

$$Z - \pi Z \approx Z_k^{(2)} - Z_k,$$
$$U - i_k u \approx U_k^{(2)} - U_k,$$

we can calculate the absolute value of the error estimator on every time interval I_m. For more details, we refer to [25]. Using the equilibration strategy presented in ([55], page 43), we are able to decide which time intervals have to be refined to get optimal convergence of the discretization in time.

Algorithm 2: Abstract adaptive algorithm using the DWR estimator

Choose initial time grid with M time intervals and max and tol
while $l <$ max or $\eta >$ tol **do**
  for $m = 1, ..., M$ **do**
    Find $U_{k,m}$ solving discretized state equation
  end for
  for $m = M, ..., 0$ **do**
    Find $Z_{k,m}$ solving discretized adjoint equation
    Evaluate η_m the a posteriori error estimator on time Interval I_m
  end for
  Determine N time intervals with large error contribution and set $\eta = \sum_{m=1}^{M} \eta_m$
  Refine the selected N time intervals and set $M = M + N$
  Set $l = l + 1$
end while

4.2. A truncation-based heuristic error indicator for goal-oriented time step control

If we are only interested in an adaptive algorithm to compute more accurately a functional of interested, which is distributed over the whole time interval, heuristic error indicators can help. For the evaluation of the DWR error estimator we have to solve one additional PDE and then recalculate on the refined time grid. A cheaper alternative can be heuristic error indicators based on the truncation error. As in the previous section, we consider a goal functional

$$\mathcal{J}(U) := \int_I j(U(t))\, \mathrm{d}t,$$

that should be computed with a certain accuracy. This accuracy is obtained by adjusting the time step size, such that the error in the functional $j(U(t))$ is below a certain threshold at every time step t_m.

We follow the idea proposed by [65] but extend the author's criterion with additional terms, which are inspired by [35, 44]. The result is a simple method but the price to pay are additional solves of the problem per time step. Specifically, per macro time step, we compute once the solution $U_{k,m}$ of our problem with step size k_m, and evaluate the goal functional $j(U_{k,m})$, and then calculate the solution $\tilde{U}$ by computing three times with time step size $\tilde{k} = \frac{k_m}{3}$ again. Afterward we compare $j(U_{k,m})$ and $j(\tilde{U})$ by evaluating the absolute error $\eta_m := |j(U_{k,m}) - j(\tilde{U})|$. If η_m is too large, we refine the time step size. An overview of the adaptive strategy is given in Algorithm 3.

Remark 4. *In general, it would be better to formulate η_m with respect to the relative error. However, this is a problem when functionals are considered that pass through the zero y-axis since then the denominator may become zero causing the entire evaluation to be infinity.*

The parameter $\gamma \approx 1$ in Algorithm 3 is a safety factor (the authors in [35] suggest to use $\gamma = 0.9$) and we chose $K = \frac{1}{15}$ as in [35]. Moreover, we implemented an additional check $k_{min} \leq k_m \leq k_{max}$ to avoid the calculation with very small or very large time step sizes. As we can see in Algorithm 3, one disadvantage of this error estimator is the selection of the model parameters γ and K, the bounds for θ (not to be confounded with the θ for the time-stepping scheme), and the choice of TOL.

Remark 5. *Keeping the step size k_m for values $1 \leq \theta \leq 1.2$ prevents high time step oscillations and we just keep the old time step if the absolute error is not too large. Several illustrating computations have been presented in [35].*

Remark 6. *As we can see, for $\theta < 0.5$ the entire calculation of the solution of this time step has to be repeated which is very expensive. However, in practice this happens rarely, but is necessary since a dramatic decrease of the time step size indicates that the current solution is by far not accurate enough.*

Algorithm 3: Abstract adaptive algorithm using the heuristic estimator

Let TOL, k_1 and U_0 be given
Set $m = 1$ and $t_1 = t_0 + k_1$
while $t_m < T$ **do**
  Given $U_{k,m-1}$ compute $U_{k,m}$ by solving one step of the discretized state equation (step size k_m)
  Set $\tilde{U}_0 = U_{k,m-1}$
  for $i = 1, 2, 3$ **do**
    Given $\tilde{U}_{i-1}$ compute $\tilde{U}_i$ by solving one step of the discretized state equation (step size $\tilde{k} = k_m/3$)
  end for
  Set $\eta_m = |j(U_{k,m}) - j(\tilde{U}_3)|$ and $\theta = \gamma \left(\frac{\mathrm{TOL}}{\eta_m} \right)^K$
  if $\theta > 0.5$ **then**
    Set $t_{m+1} = t_m + k_m$ and $m = m + 1$
  end if
  if $\theta < 1$ or $\theta > 1.2$ **then**
    Set $k_m = \theta k_m$
  end if
end while

5. On the Adjoint Equation

To evaluate the DWR error estimator presented in Section 4.1, we must calculate local sensitivity information of the FSI problem with respect to the functional of interest. To do so we have to derive the adjoint equation. In this section, we explain the procedure and focus on non-standard aspects while providing some examples.

5.1. Time discretization

The evaluation of the residual based DWR error estimator expects the solution of the adjoint problem

Problem 10. *(Adjoint FSI Problem) Find $Z \in \tilde{X}$ solving the adjoint equation*

$$A'(U)(\Phi, Z) = \mathcal{J}'(U)(\Phi) \quad \forall \Phi \in X.$$

Thereby, we have to calculate the directional derivative of the semi-linear form $A(U)(\Phi)$ with respect to $U = (u, v, p)$. The resulting linearized form in each discrete time point is first used as left hand side in Newton's method (i.e., the Jacobian). Second, we obtain the adjoint equation by switching test and trial functions. The latter one reads in more detail:

Problem 11. *Find $(z^v, z^u, z^p) \in L^2(I; V^v) \times L^2(I; V^u) \times L^2(I; L_f)$ such that*

$$\begin{aligned}
A'_{F,v}(U)(\varphi, z^v) + A'_{S,v}(U)(\varphi, z^v) + A'_{V,v}(U)(\varphi, z^u) + A'_{D,v}(U)(\varphi, z^p) & \\
+ A'_{\Gamma,v}(U)(\varphi, z^v) + I'_{V,v}(U)(\varphi, z^v) = \mathcal{J}'_v(U)(\varphi) \quad & \forall \varphi \in L^2(I; V^v), \\
A'_{F,u}(U)(\psi, z^v) + A'_{S,u}(U)(\psi, z^v) + A'_{V,u}(U)(\psi, z^u) + A'_{M,u}(U)(\psi, z^u) & \\
+ A'_{D,u}(U)(\psi, z^p) + A'_{\Gamma,u}(U)(\psi, z^v) + F'_u(U)(\psi, z^v) + I'_{U,u}(U)(\psi, z^v) = \mathcal{J}'_u(U)(\psi) \quad & \forall \psi \in L^2(I; V^u), \\
A'_{F,p}(U)(\xi, z^v) = \mathcal{J}'_p(U)(\xi) \quad & \forall \xi \in L^2(I; L_f).
\end{aligned}$$

We refer the reader to the appendix of the stated semi-linear forms. As already in the previous Section 3.1, we replace the continuous spaces by the suggested time discrete spaces X_k and $X_{k,\theta}$. Therefore, the Petrov-Galerkin semi-discretized adjoint problem writes as

Problem 12. *Find $(z^v_k, z^u_k, z^p_k) \in W^v_{k,\theta} \times W^u_{k,\theta} \times W^p_k$ such that*

$$A'(U_k)(\Phi_k, Z_k) = \mathcal{J}'(U_k)(\Phi_k) \quad \forall \Phi \in X_k. \tag{12}$$

As test and trial spaces have been switched in the adjoint equation, the adjoint solutions z_k^v and z_k^u are now elements of the θ dependent space $W_{k,\theta}^v$ and $W_{k,\theta}^u$. Every test function $(\varphi_k, \psi_k, \xi_k) \in W_k^v \times W_k^u \times W_k^p$ can be presented as

$$\varphi_k = \sum_{i=0}^{N} \varphi_m \omega_m(t), \quad \psi_k = \sum_{i=0}^{N} \psi_m \omega_m(t), \quad \xi_k = \sum_{i=1}^{N} \mathcal{X}_{I_m}(t) \xi_m,$$

with $(\varphi_m, \psi_m, \xi_m) \in V^v \times V^u \times L_f$, too. Whereby ω_m is again a hat function on the given time grid as given in Figure 2. To evaluate the time integrals in the adjoint equation we use the possibility to write functions in $W_{k,\theta}^v \times W_{k,\theta}^u \times W_k^p$ as linear combination of $\omega_{m,\theta}$ and $\mathcal{X}_{I_m}$. We get

$$z_k^v = \sum_{i=0}^{M} z_{k,m}^v \omega_{m,\theta}(t), \quad z_k^u = \sum_{i=0}^{M} z_{k,m}^u \omega_{m,\theta}(t) \quad \text{and} \quad z_k^p = \sum_{i=1}^{M} z_{k,m}^p \mathcal{X}_{I_m}(t)$$
$$\text{with} \quad z_{k,m}^v := \frac{1}{k_m} \int_{I_m} z_k^v \mathrm{d}t, \quad z_{k,m}^u := \frac{1}{k_m} \int_{I_m} z_k^u \mathrm{d}t \quad \text{and} \quad z_{k,m}^p := \frac{1}{k_m} \int_{I_m} z_k^p \mathrm{d}t.$$

Applying again the suggested quadrature rule (2) and exploiting the linearity of the equation (12) with respect to the test functions, results again in a time stepping scheme.

Remark 7. *We emphasize that for optimal control of fluid-structure interaction problems the same adjoint equation has to be computed. Hence specifically there, the adaptive algorithm pays of, as the adjoint information is already known.*

5.2. Examples of adjoint FSI equations

To illustrate how the time stepping scheme can be realized, we evaluate the integral terms occurring in the m-th dual step in the adjoint transport term as an example. We apply the quadrature rule on the time interval I_m yielding

$$\begin{aligned}
&\int_{I_m} (\rho_f^0 J_k (F_k^{-1}(v_k - \partial_t u_k) \cdot \nabla)\omega_m(t)\varphi_m), z_{k,m}^v \omega_{m,\theta})_f \, \mathrm{d}t = \\
&k_m \theta_m ((\rho_f^0 J_k(t_m^-)(F_k^{-1}(t_m^-)(v_k(t_m^-) - \partial_t u_k(t_m^-)) \cdot \nabla)\omega_m(t_m^-)\varphi_m, z_{k,m}^v)_f \\
+k_m(1-\theta_m)&((\rho_f^0 J_k(t_{m-1}^+)(F_k^{-1}(t_{m-1}^+)(v_k(t_{m-1}^+) - \partial_t u_k(t_{m-1}^+)) \cdot \nabla)\omega_m(t_{m-1}^+)\varphi_m, z_{k,m}^v)_f \\
&= k_m \theta_m ((\rho_f^0 J_{k,m}(F_{k,m}^{-1}(v_{k,m} - \frac{u_{k,m} - u_{k,m-1}}{k_m}) \cdot \nabla)\varphi_m, z_{k,m}^v)_f.
\end{aligned}$$

Similarly we obtain on the time interval I_{m+1}

$$\begin{aligned}
&\int_{I_{m+1}} (\rho_f^0 J_k (F_k^{-1}(v_k - \partial_t u_k) \cdot \nabla)\omega_m(t)\varphi_m), z_{k,m+1}^v \omega_{m+1,\theta})_f \, \mathrm{d}t = \\
k_{m+1}\theta_{m+1}&((\rho_f^0 J_k(t_{m+1}^-)(F_k^{-1}(t_{m+1}^-)(v_k(t_{m+1}^-) - \partial_t u_k(t_{m+1}^-)) \cdot \nabla)\omega_{m+1}(t_{m+1}^-)\varphi_m, z_{k,m+1}^v)_f \\
+k_{m+1}(1-\theta_{m+1})&((\rho_f^0 J_k(t_m^+)(F_k^{-1}(t_m^+)(v_k(t_m^+) - \partial_t u_k(t_m^+)) \cdot \nabla)\omega_m(t_m^+)\varphi_m, z_{k,m+1}^v)_f \\
&= k_{m+1}(1-\theta_{m+1})((\rho_f^0 J_{k,m}(F_{k,m}^{-1}(v_{k,m} - \frac{u_{k,m+1} - u_{k,m}}{k_{m+1}}) \cdot \nabla)\varphi_m, z_{k,m+1}^v)_f.
\end{aligned}$$

As ω_m has compact support only on the time intervals I_m and I_{m+1} we obtain

$$\begin{aligned}
&\int_I (\rho_f^0 J_k (F_k^{-1}(v_k - \partial_t u_k) \cdot \nabla)\omega_m(t)\varphi_m), z_k^v)_f \, \mathrm{d}t = \\
&k_m \theta_m ((\rho_f^0 J_{k,m}(F_{k,m}^{-1}(v_{k,m} - \frac{u_{k,m} - u_{k,m-1}}{k_m}) \cdot \nabla)\varphi_m, z_{k,m}^v)_f \\
+k_{m+1}(1-\theta_{m+1})&((\rho_f^0 J_{k,m}(F_{k,m}^{-1}(v_{k,m} - \frac{u_{k,m+1} - u_{k,m}}{k_{m+1}}) \cdot \nabla)\varphi_m, z_{k,m+1}^v)_f.
\end{aligned}$$

As we can see, to calculate the adjoint solution Z_m, we need the adjoint solution Z_{m+1} from the previous time-step. Therefore, the adjoint equation runs backward in time. But in contrast to the forward problem the adjoint time stepping scheme depends on θ_m and θ_{m+1} and on the solution U_{m-1}, U_m and U_{m+1}. The adjoint time stepping scheme, therefore has not the same structure as the theta scheme of the forward problem. As the adjoint equation is not autonomous we do not integrate the adjoint equation first in time before replacing the continuous spaces with its discrete equivalent. Therefore, we have to evaluate terms with the time derivative of the test function. We just exploit the fact that $\partial_t \omega_m|_{I_m} = \frac{1}{k_m}$, $\partial_t \omega_m|_{I_{m+1}} = \frac{1}{k_{m+1}}$ and zero elsewhere. Using the same techniques as before we obtain for example

$$\begin{aligned}
&\int_I -(\rho_f^0 J_k (F_k^{-1} \partial_t \omega_m(t) \psi_m \cdot \nabla) v_k), z_k^v)_f \, \mathrm{d}x = \\
&-((1-\theta_m)\rho_f^0 J_{k,m-1}(F_{k,m-1}^{-1}\psi_m \cdot \nabla) v_{k,m-1} + \theta_m \rho_f^0 J_{k,m}(F_{k,m}^{-1}\psi_m \cdot \nabla) v_{k,m}, z_{k,m}^v)_f \\
&+((1-\theta_{m+1})\rho_f^0 J_{k,m}(F_{k,m}^{-1}\psi_m \cdot \nabla) v_{k,m} + \theta_{m+1} \rho_f^0 J_{k,m+1}(F_{k,m+1}^{-1}\psi_m \cdot \nabla) v_{k,m+1}, z_{k,m+1}^v)_f.
\end{aligned}$$

Note that first and last step of the adjoint equation look slightly differently. The linearization of the functional of interest in the right-hand side of the dual equation is again approximated using the θ dependent quadrature rule (2).

5.3. Adjoint divergence condition

The average divergence condition causes an "average adjoint pressure term". As we changed the divergence condition in Section 3.2, we have to adapt the adjoint time-stepping scheme to get a consistent formulation. Therefore we replace the adjoint pressure dependent terms

$$\begin{aligned}
A'_{D,v}(p,v,u)(\varphi, z_{k,m}^p) =& k_m(\mathrm{div}(J_{k,m}F_{k,m}^{-1}\varphi), z_{k,m}^p))_f \\
&+ k_{m+1}(\mathrm{div}(J_{k,m}F_{k,m}^{-1}\varphi), z_{k,m+1}^p))_f \\
A'_{D,u}(p,v,u)(\psi, z_{k,m}^p) =& k_m(\mathrm{div}(J_{k,m}\,\mathrm{tr}(F_{k,m}^{-1}\nabla\psi)F_{k,m}^{-1}v_{k,m}), z_{k,m}^p))_f \\
&+ k_{m+1}(\mathrm{div}(J_{k,m}\,\mathrm{tr}(F_{k,m}^{-1}\nabla\psi)F_{k,m}^{-1}v_{k,m}), z_{k,m+1}^p))_f \\
&- (\mathrm{div}(J_{k,m}F_{k,m}^{-1}\nabla\psi F_{k,m}^{-1}v_{k,m}), z_{k,m}^p)_f \\
&- k_{m+1}(\mathrm{div}(J_{k,m}F_{k,m}^{-1}\nabla\psi F_{k,m}^{-1}v_{k,m}), z_{m+1}^p)_f,
\end{aligned}$$

by the terms

$$\begin{aligned}
A'_{D,v}(p,v,u)(\varphi, z_{k,m}^p) =& k_m(\mathrm{div}(J_{k,m}F_{k,m}^{-1}\varphi), z_{k,m}^p))_f \\
A'_{D,u}(p,v,u)(\psi, z_{k,m}^p) =& k_m(\mathrm{div}(J_{k,m}\,\mathrm{tr}(F_{k,m}^{-1}\nabla\psi)F_{k,m}^{-1}v_{k,m}), z_{k,m}^p))_f \\
&- (\mathrm{div}(J_{k,m}F_{k,m}^{-1}\nabla\psi F_{k,m}^{-1}v_{k,m}), z_{k,m}^p)_f.
\end{aligned}$$

Thereby the adjoint pressure is given in a fully implicit fashion. Therefore, the semi-discretized adjoint and semi-discretized-state equations match again.

6. Numerical Tests

In this section, we present several numerical examples to investigate the performance of our algorithms. In Example 1, utilizing the FSI-3 benchmark [41, 14, 13], we perform a computational analysis with respect to certain goal functionals of four popular time-stepping schemes. We are specifically interested in the stability and accuracy of these schemes for large time steps since our adaptive algorithms allow for both time grid refinement and coarsening. In the second and third tests, we turn our attention to adaptive time step control considering the FSI-3 and FSI-2 benchmarks. We compute them with the originally proposed inflow profile[1] and also with a modified inflow profile. In the latter one, we decrease the inflow (after full oscillations have been developed) in order to study how the error estimator can deal with time step refinement and coarsening. In the fourth example, we consider a flapping test proposed in [31] inspired by hemodynamics. To strengthen our findings, we provide computations in two different software packages, i.e., RoDoBo [60] and the FSI-template [70] based on deal.II [3, 4].

[1]The results for FSI-2 are not shown here, because they have been well investigated in the literature for uniform time steps.

6.1. Setups

We first provide details on geometries, boundary conditions, parameters, and quantities of interest.

Configuration. The geometry of the FSI-3 and FSI-2 settings are displayed in Figure 3. An elastic beam is attached to a cylinder and is surrounded by an incompressible fluid.

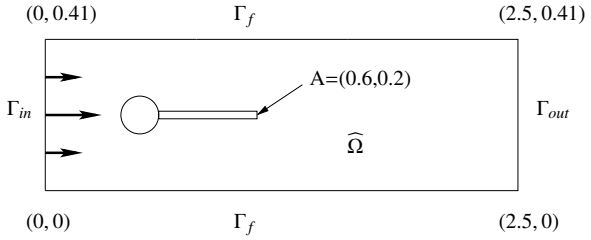

Figure 3: FSI-2 and FSI-3 benchmarks (Examples 1-3): flow around cylinder with elastic beam with circle-center $C = (0.2, 0.2)$ and radius $r = 0.05$.

On the cylinder and outer boundary Γ_f we enforce zero Dirichlet boundary conditions. On the outflow boundary Γ_{out} we prescribe the do-nothing outflow condition [38]. The inflow profile on Γ_{in} is given by:

$$v(0, y) := 1.5y(0.41 - y)\frac{4}{0.41^2}v_{mean}(t).$$

The mean inflow $v_{mean}(t)$ is specified in each respective subsection below. We regard the time intervals $I = [0, 12s]$ (FSI-3) and $I = [0, 25s]$ (FSI-2). The material parameters are chosen as proposed in [41, 14, 13] and listed in Table 1 (therein the parameters for the flapping membrane test, Example 4, are listed, too).

	FSI-2	FSI-3	Flapping
ν_f	$10^{-3}\frac{m^2}{s}$	$10^{-3}\frac{m^2}{s}$	$10^{-1}\frac{m^2}{s}$
λ_s	$0.5 \cdot 10^6\frac{kg}{ms^2}$	$2 \cdot 10^6\frac{kg}{ms^2}$	$2.0 \cdot 10^7\frac{kg}{ms^2}$
μ_s	$2.0 \cdot 10^6\frac{kg}{ms^2}$	$8.0 \cdot 10^6\frac{kg}{ms^2}$	$8.0 \cdot 10^7\frac{kg}{ms^2}$
ν_m	-0.1	-0.1	-0.1
ρ_s^0	$10^4\frac{kg}{m^3}$	$10^3\frac{kg}{m^3}$	$10^2\frac{kg}{m^3}$
ρ_f^0	$10^3\frac{kg}{m^3}$	$10^3\frac{kg}{m^3}$	$10^2\frac{kg}{m^3}$

Table 1: Material parameters for all test cases.

Quantities of interest / goal functionals for all test cases (Examples 1-4). To compare the computed solutions on different time-meshes we evaluate several time dependent functionals. As in [41, 14, 13], we calculate the four quantities of interest at each (discrete) time point: the displacements in both the x- and y-directions at the point $A = (0.6, 0.2)$ and the drag/lift values over the cylinder boundary and FSI-interface:

$$\int_{\Gamma\cup\Gamma_{cyl}} -\sigma_f n e_i \,\mathrm{d}x, \quad i = 1, 2.$$

For the error estimation, we integrate the values over time to have a functional value which can easily be compared:

$$\mathcal{J}_1(U) := \int_I u_x^2(t)\,\mathrm{d}t, \quad \mathcal{J}_2(U) := \int_I u_y^2(t)\,\mathrm{d}t.$$

In addition we calculate the drag over time:

$$\mathcal{J}_3(U) := \int_I \int_{\Gamma \cup \Gamma_{cyl}} -\sigma_f n e_1 \, \mathrm{d}x \, \mathrm{d}t.$$

A further characteristic value for the fluid is the vorticity. Due to boundary layers we use the Okubo-Weiss criterion, which was first introduced in [52, 66]. The vorticity is given as the positive value of $\det(\nabla v)$. Due to the moving domain we have to transform the criteria on the reference domain. To be able to calculate sensitivities of the functional we use the regularized version

$$\mathcal{J}_4(U) := \int_{\Omega_f} \int_I Jg\Big(det(\nabla v F^{-1})\Big) \, \mathrm{d}t, \quad \text{with} \quad g(x) = \begin{cases} 0 & , x < 0 \\ \frac{t^3}{1+t^2} & , x > 0, \end{cases}$$

suggested in [46]. In addition to the functional evaluation on the entire fluid domain we calculate the vorticity value in the area $\tilde{\Omega}_f := \{v \in \Omega_f | \; x > 0.9\}$ behind the elastic beam

$$\mathcal{J}_5(U) := \int_{\tilde{\Omega}_f} \int_I Jg\Big(det(\nabla v F^{-1})\Big) \, \mathrm{d}t.$$

6.2. Example 1: A comparison of four time stepping schemes in terms of the FSI-3 benchmark

Before we begin with detailed comparisons of adaptivity and the two proposed adaptive time step control schemes (see Section 4), we briefly motivate our choice to work with the Fractional-Step-theta scheme. To this end, we perform a computational analysis in which we compare the behavior of the 2nd order A-stable Crank-Nicolson scheme ($\theta_m = 0.5$), the 2nd order strictly stable shifted Crank-Nicolson scheme ($\theta_m = 0.5 + k_s$), the 2nd order Rannacher scheme (RR10), and the Fractional-Step-theta (FSTheta) scheme. In the Rannacher scheme, we apply every 10th time step a backward Euler step. For these comparisons we utilize the FSI-3 benchmark.

Discussion of our findings. Only the last three schemes are known to work well for Navier-Stokes flow on its own (see e.g., [61, 44, 37]). For fluid-structure interaction we observe that the Rannacher scheme is stable, but yields inaccurate drag and lift values. This is an important observation since in flow applications, one is in particular interested in the accurate evaluation of such boundary forces. As shown in [67], for FSI-2, the shifted Crank-Nicolson and Fractional-Step-theta scheme both work well. However, one drawback of the shifted Crank-Nicolson scheme is the determination of the shift value $k_s \approx k_m$ because it must hold $k_m < 0.5$, since otherwise $\theta \in [0, 1]$ is violated. Moreover, on adaptively refined time grids it is unclear how the shift value has to be chosen to preserve sufficient smoothing, but to avoid a notable influence on the physical numerical solution. For the FSI-3 benchmark such comparisons have not yet been made in existing studies.

As implicit time-stepping schemes allow for large time steps, we choose $k_m = 0.01s$ such that the dynamics of the FSI configuration can barely be resolved. We observe that both the original Crank-Nicolson and the shifted version will fail after some time. On the other hand, both the Rannacher and Fractional-Step-theta schemes yield satisfactory results for the y-displacements. However, for the drag evaluation, the Rannacher scheme exhibits numerical instabilities as shown in Figure 5. In view of these findings, we conclude that employing large time steps, the Fractional-Step-theta scheme seems to be the optimal choice as time stepping scheme. For smaller time steps, we expect all time-stepping schemes to work as it is well-known that then the numerical stability increases. However, the main purpose of our investigation is time grid coarsening. Both algorithms in Section 4 do explicitly allow for large time steps in case the error estimator predicts larger steps. Here, it is important to have a stable algorithm such that numerical errors do not accumulate. According to our findings in this section, these requirements are best fulfilled by the Fractional-Step-theta scheme.

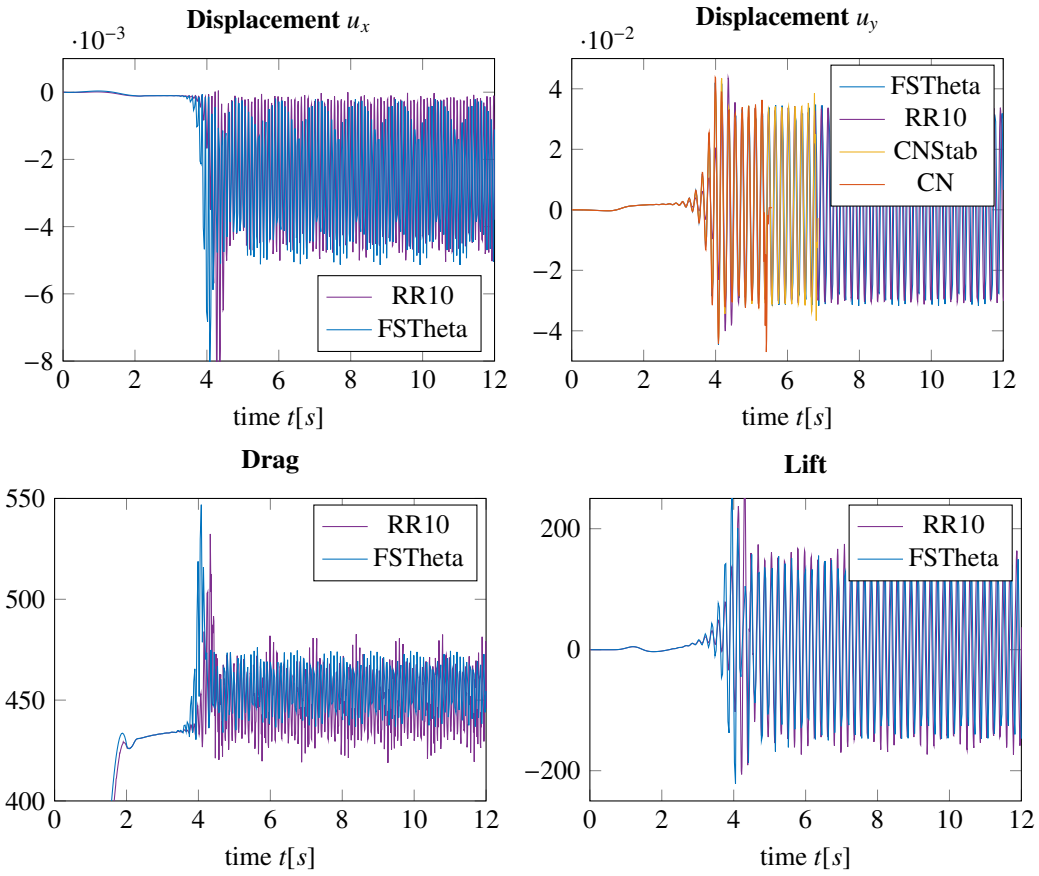

Figure 4: Section 6.2, FSI 3: Comparison of various time-stepping schemes showing blow-up for the two Crank-Nicolson schemes in both the u_y displacements and the drag values at $T = 5.5s$ and $T = 6.8s$, respectively. The Rannacher time stepping (using Crank-Nicolson and smoothing every 10th step, respectively, with backward Euler), works more stable, but also shows numerical irregularities in the drag values. The Fractional-Step-theta scheme is the most stable scheme. This is widely known in the literature, but for fluid-structure interaction such a computational analysis has been not available yet in the literature.

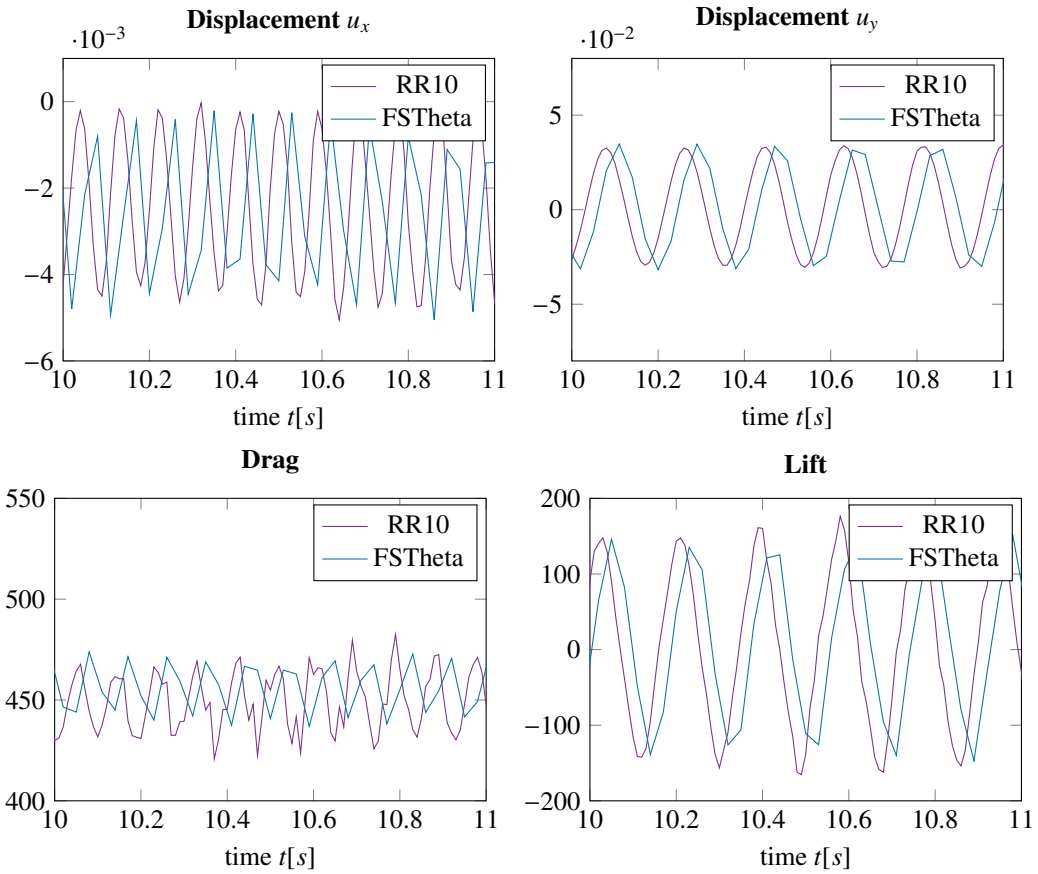

Figure 5: Section 6.2, FSI 3: Zoom-in to the four quantities of interest. In the drag evaluation employing the Rannacher scheme, we observe numerical instabilities represented by additional smaller oscillations after the smoothing Euler step.

6.3. Example 2: Adaptive solution of the FSI-3 benchmark

In this section, we turn our attention to adaptivity. We begin with the FSI-3 benchmark because this example is easier in the sense that the deflections of the elastic flag are less in comparison to FSI-2.

To avoid artificial oscillations and large numerical errors the authors in [41] suggest to increase smoothly the inflow velocity. In the following we choose an inflow profile, which lacks this regularity to test if our adaptive algorithms are able to tackle the kinks in the mean inflow. In addition the mean inflow velocity

$$v_{mean}(t) = \begin{cases} 0.5t & , t \leq 2 \\ 1 & , t > 2, t \leq 6 \\ 4 - 0.5t & , t > 6, t \leq 7 \\ 0.5 & , else \end{cases}$$

decreases again after full oscillations have been developed, to enforce varying dynamics over time.

In Figure 6 we plotted the displacement at the tip of the flag and the drag value over time. As in the standard FSI-3 benchmark the beam starts to oscillate after some time, whereby frequency and amplitude are equivalent to the standard benchmark for $t < 6$. The moment the inflow decreases, the amplitude of the oscillations reduces and the configuration converges to a steady state. This behavior also can be seen in the drag value. We also notice that in both codes, the two functionals in the time interval $[4, 6]$ are around the limits of the published benchmark results (e.g., [13]). The RoDoBo solutions show a slightly larger amplitude which may be due to the LPS-stabilization.

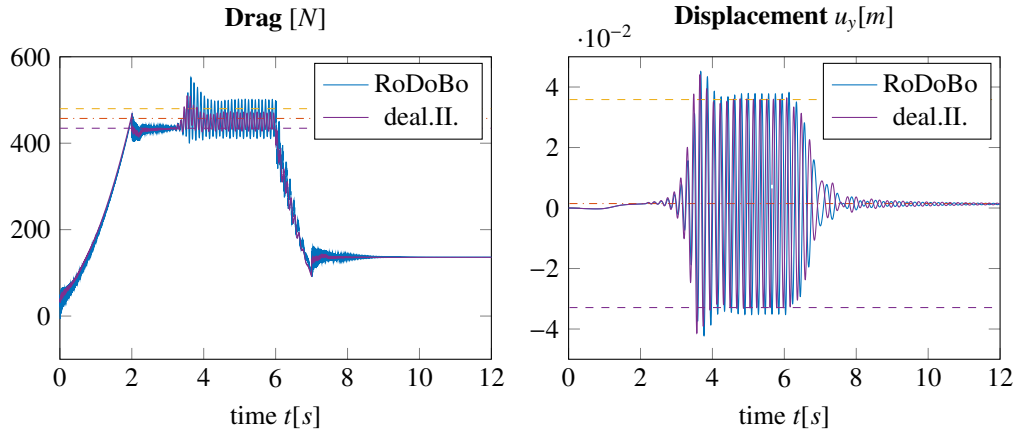

Figure 6: Solution of the FSI-3 benchmark using the new inflow profile. Drag value at the flag and cylinder (left) and displacement u in y-direction at the tip of the flag (right) plotted over time t.

6.3.1. Functional of interest: vorticity

To compare the accuracy of the computed solution we choose the vorticity functional $\mathcal{J}_5$ defined in the second half of the the cylinder. The error in the functional of interest due to time discretization is plotted in Figure 7 over the number of time steps. The space discretization is kept constant. As reference value for the functional we use the solution on a very fine equidistant time grid with $M = 144\,384$ time steps. The error in the functional of interest thereby converges slightly faster using the adaptive algorithm, with the DWR error estimator as refinement indicator, compared to global refinement in time. In addition, the DWR error estimates of the time discretization error are quite close to the exact values of the error. For the chosen parameters the heuristic error estimator reduces the error in the functional of interest by a similar factor.

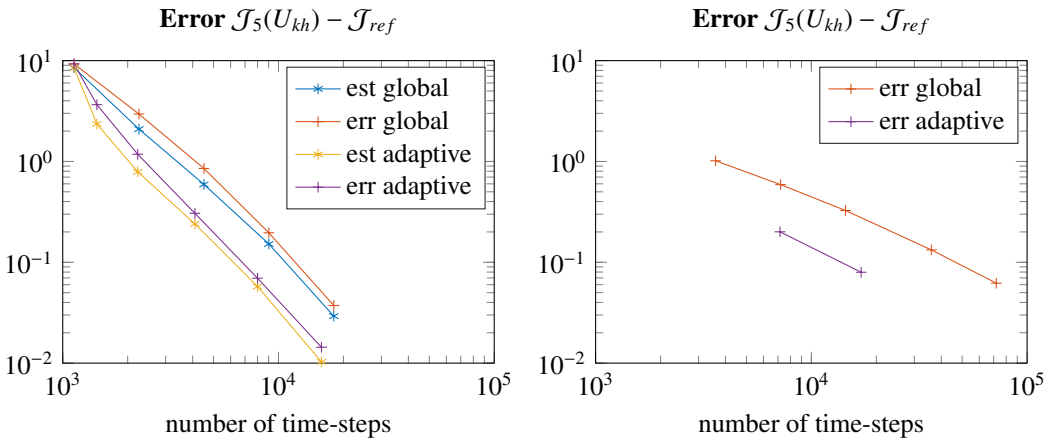

Figure 7: Section 6.3.1: Error in the vorticity functional for the FSI-3 benchmark . Here a comparison between uniform refinement, the DWR estimator, the DWR error (left) and the heuristically obtained adaptive steps (right) is provided. With regard to the complexity of this nonlinear FSI problem, we observe excellent behavior w.r.t. to the effectivity index as well as comparing the DWR and heuristic errors. Second, we clearly observe that adaptive grid refinement pays off in this setting (in contrast to the results shown in Figure 10). The results in the left figure are computed in RoDoBo and in the right figure with deal.II.

6.3.2. Functional of interest: drag

Furthermore we evaluate the functional $\mathcal{J}_3(U)$, measuring the drag around the cylinder and the beam. To evaluate the error estimator, it is reasonable to compare the effectivity indices I_{eff}. The effectivity index is defined as quotient of the DWR time discretization error estimator and exact discretization error $\mathcal{J}_{ref} - \mathcal{J}(U_{kh})$. As reference value, we use again the solution on a very fine equidistant time grid with $M = 1\,444\,384$ time steps.

DoFs in time	1128	2256	4512	9024	18048	36096
I_{eff}	0.86	0.84	0.94	1.35	0.69	1.18

Table 2: Section 6.3.2: Effectivity indices I_{eff} for DWR time discretization error estimator with respect to $\mathcal{J}_3(U)$ on globally refined time grids.

DoFs in time	1128	1458	2310	4122	4890	7440	9420	9420
I_{eff}	0.86	0.84	0.94	1.98	2.85	0.89	0.86	0.88

Table 3: Section 6.3.2: Effectivity indices I_{eff} for DWR time discretization error estimator with respect to $\mathcal{J}_3(U)$ on adaptively refined time grids.

The effectivity indices are very close to one. Therefore the error in the functional of interest is neither overestimated nor underestimated. Therefore the error estimator can be used in addition as stopping criteria for the simulation. Furthermore if error estimates for the space discretization are available, the error estimator enables us to decide if it is necessary to refine in space and time or just in one of the two.

To achieve a fast converging adaptive algorithm it is also important to have an accurate localization of the error to know where to refine the time grid. In Figure 8 we plotted the time step size over time after 1, 3 and 6 refinement steps. The DWR algorithm refines the areas where the beam oscillates with fast frequency as we would expect. In addition the adaption strategy does not refine the time grid for $t > 8$, when the solution converges against a stationary solution. Surprisingly the algorithm refines quite heavily at the beginning. But if we take a closer look to the drag values in Figure 6, we can see that the fast increasing inflow causes oscillations in the drag value.

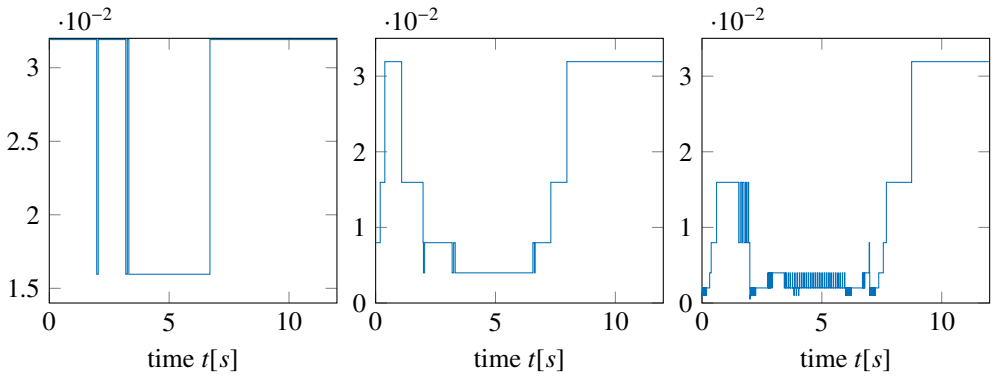

Figure 8: Section 6.3.2: time step size k_m plotted over time t after 1 (left), 3 (middle) and 6 (right) adaptive refinements for the FSI-3 benchmark using the DWR time discretization error estimator with respect to $\mathcal{J}_3(U)$.

6.4. Example 3: Adaptive solution of the FSI-2 benchmark

The geometry for the FSI-2 benchmark is identical to the FSI-3 benchmark as displayed in Figure 3. But as the solid Lamé parameters and maximum inflow are both smaller, the beam starts to oscillate with lower frequency, but with higher amplitude. As in the previous simulations, we choose an inflow profile rising linearly. After some constant period, the inflow profile

$$v_{mean}(t) = \begin{cases} 0.5t & ,t \leq 2 \\ 1 & ,t > 2, t \leq 14 \\ 8 - 0.5t & ,t > 14, t \leq 15 \\ 0.5 & ,else \end{cases}$$

decreases again.

Discussion of our findings. In Figure 9 we plot the displacement at the tip of the flag at the point $A = (0.6, 0.2)$ over time. In comparison to the FSI-3 configuration (see Figure 6) the damping of the beam due to the fluid flow is much slower. In the time frame $t \in [10, 14]$ the frequency and amplitude coincide with the reference values of the standard FSI-2 benchmark.

To analyze the convergence rate of the Fractional-Step-theta time stepping scheme we plot in Figure 10 the functional $\mathcal{J}_2(U)$, the displacement at the tip in y-direction integrated over time. Here we compute a reference solution again on a fine time grid with $M = 149\,760$ Fractional-Step-theta time steps. Due to the lower inflow velocity, the solution is smoother in time in comparison to the FSI-3 benchmark. In addition even at the end time point T the solution has not reached a steady state. That is why global refinement is reasonable here. Therefore, the adaptive algorithm does not provide any advantages with respect to convergence in time. This example demonstrates nicely that adaptivity works, but is not favored in this setting. For instance when we know in advance that the solution is regular enough all the efforts in evaluating the adjoint problem can be saved by just using uniform time grid refinement. In the right subfigure of Figure 10, we observe our findings obtained with the deal.II code. For global time grid refinement, we observe (as expected) a very similar behavior as seen for the first code. The heuristic error estimator performs less well. The error in the goal functional values is reduced, but the order of convergence is not as good as using DWR time grid refinement.

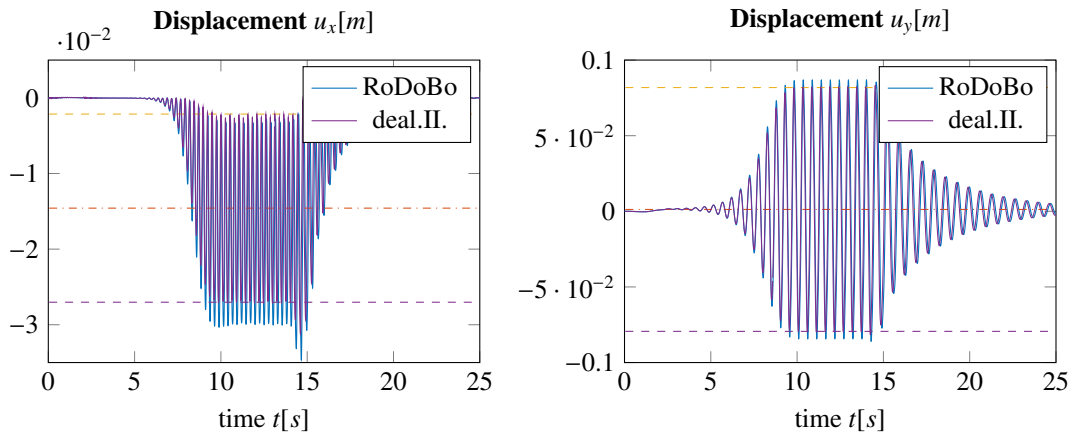

Figure 9: Section 6.4: Solution of the FSI-2 benchmark using the new inflow profile. Displacement u in x-direction (left) and y-direction (right) at the tip of the flag plotted over time. As in Figure 6, we notice that the RoDoBo solutions show a slightly larger amplitude, in particular for the displacement in x direction, which may be again due to the LPS-stabilization. Apart from this difference, both codes deliver excellent results and agreements with the published literature (e.g., [41, 68]).

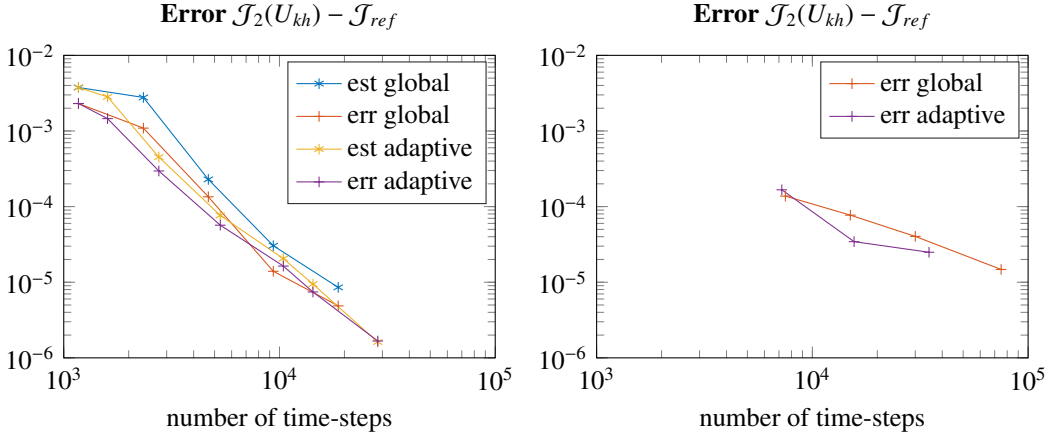

Figure 10: Section 6.4: Error in the functional $\mathcal{J}_2(U)$ for the FSI-2 benchmark plotted over the number of time steps (left RoDoBo using DWR and at right deal.II with the heuristic estimator). From these results, we first observe that the heuristic estimator performs worse than DWR in terms of the convergence order in time. Second, adaptive time grid refinement does not yield benefits, which is very likely due to the smoothness of the inflow profile and the entire numerical solution.

6.5. Example 4: Flapping membranes

In this final example, we consider a setting which is motivated by hemodynamics applications [31]. Originally, this configuration was developed to test alternative methods to ALE fluid-structure interaction as used in this paper. Indeed the elastic flaps undergo very large deformations. In more detail, a fluid in a channel flows through the gap between two vertical beams (see Figure 11) whereby the fluid flow induces a flapping of the two beams. The material parameters are provided in Table 1.

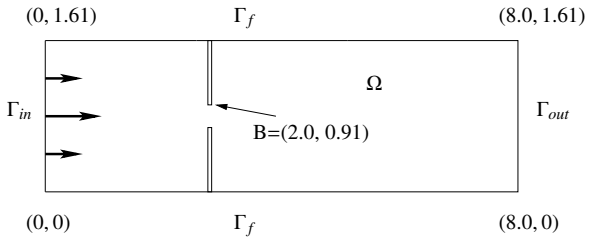

Figure 11: Flow through two elastic beams.

On the inflow boundary Γ_{in} we prescribe a parabolic inflow profile

$$v(0, y) := 1.5y(1.61 - y)\frac{4}{1.61^2}v_{mean}(t) \quad \text{for } t \in I := [0, 0.9],$$

where $v_{mean}(t)$ taken from Figure 12 (as used for similar simulations in [71]).

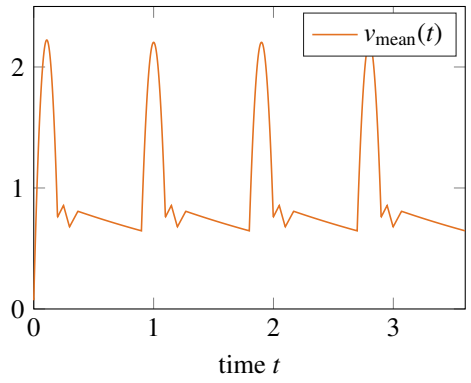

Figure 12: Interpolated flow rate profile $\bar{v}(t)$, representative of a blood flow rate in one cardiac cycle that is used to scale the inflow profile.

As in the FSI benchmark we enforce zero Dirichlet boundary conditions on the outer boundary Γ_{Wall} and a do-nothing outflow condition on the outflow boundary Γ_{out}. The computations are performed on the time interval $I = [0, 3.6s]$. Here, the time interval $[0, 0.9s]$ is periodically extended such that 4 cycles are computed. In this example, an adjusted distributed Young's modulus in the mesh motion equation has been implemented in RoDoBo, while in deal.II we employ the biharmonic model from [68].

Discussion of our findings. For very large inflow velocities, the algorithm fails as the mesh motion equation cannot be solved anymore due to the large displacements of the beam. Therefore the maximal value of parabolic inflow profile is chosen in such a way, that the mesh motion still can be handled, which however yields findings that are very good for ALE-FSI.

To visualize the behavior of the given configuration we plotted the displacement of the flag at the point $B = (2.0, 0.91)$, the drag around the two beams, and the vorticity over time in Figure 15. Due to the varying inflow, the

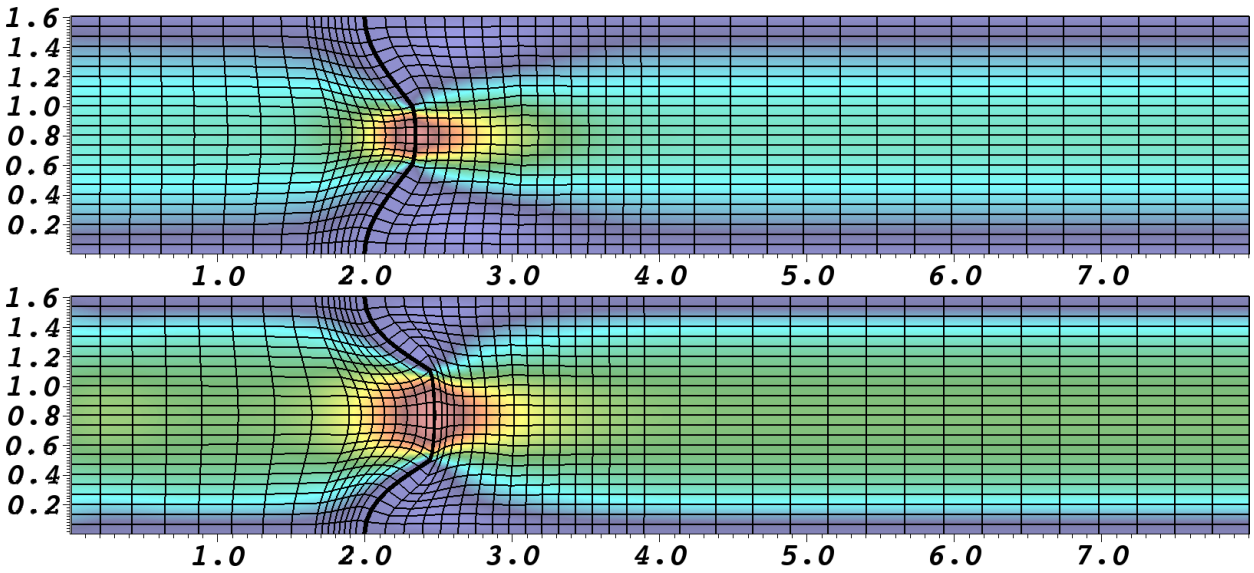

Figure 13: Example 4: Velocity field and mesh deformation at two time steps $T = 0.9s$ and $T = 1.0725s$ using the biharmonic mesh motion model.

beams are at rest at some points and the moment the inflow profile increases the gap between the beams rises. In addition, the change in the fluid velocity induces large changes in the drag and vorticity values.

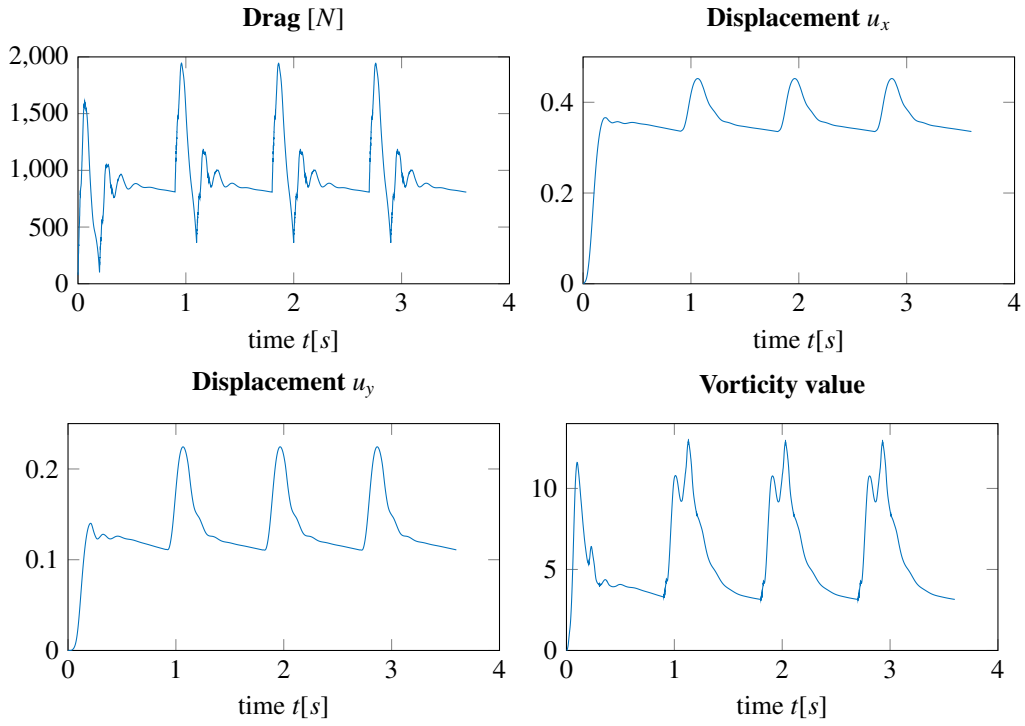

Figure 15: Section 6.5: Solution of the flapping test. Drag around the beam (upper left), displacement at the point B in x-direction (upper right) and y-direction (lower left) as well as the vorticity value (lower right) plotted over time.

As in the previous configuration we evaluate a functional of interest to compare the temporal discretization error.

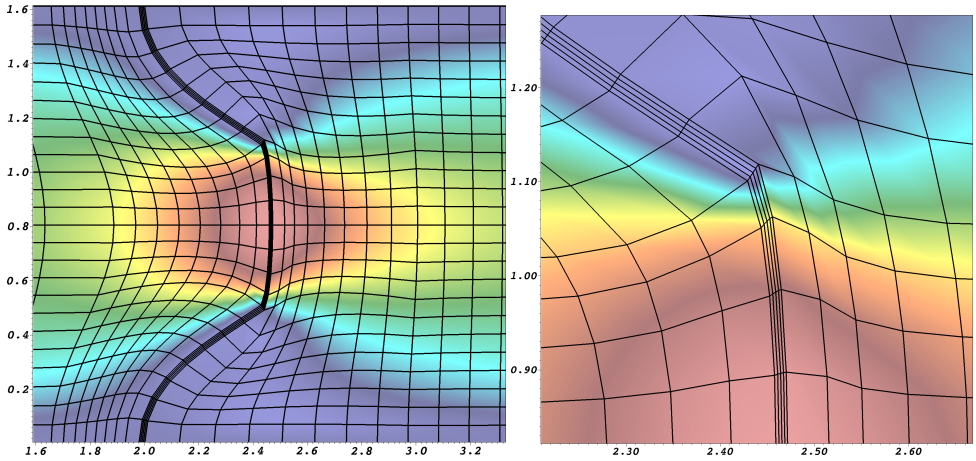

Figure 14: Example 4: Focusing on the thin elastic flaps and mesh deformation at the highest deformation at $T = 1.0725s$.

Here we choose the vorticity functional $\mathcal{J}_4(U)$. A reference value is computed on a fine grid with $M = 92\,160$ time steps. First we solve the configuration on different time grids. Then we use the DWR error estimator to refine the time grid adaptively. As we can see in Figure 16 the adaptive algorithm converges much faster in comparison to the globally refined time grid.

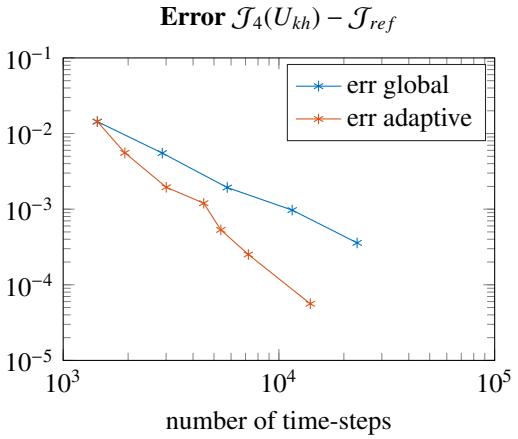

Figure 16: Section 6.5: Errors in the vorticity functional for the flapping test plotted over number of time steps.

Again we plot the resulting time steps after 1, 3 and 6 refinement steps over time in Figure 17. The adaptive algorithm refines very locally in the areas of large inflow velocity but also identifies the kinks in the inflow profile and refines there. The heuristic error estimator indicates the same regions with high inflow velocity and adapts the time-step size in a similar fashion as the DWR algorithm as we can see in Figure 18.

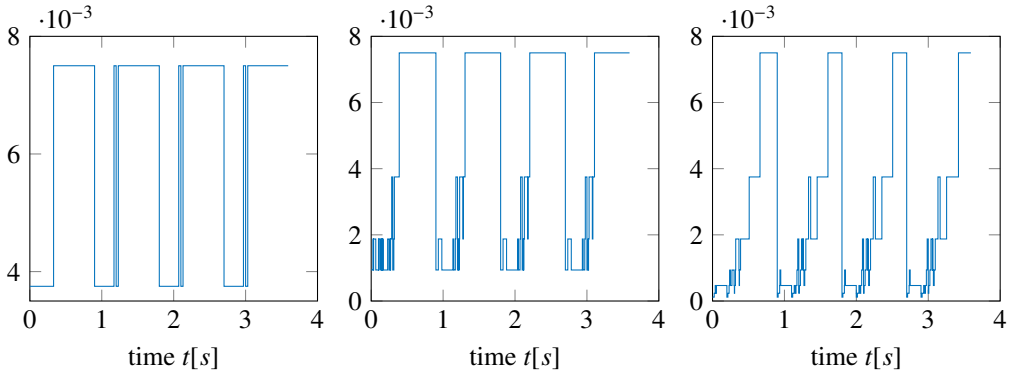

Figure 17: Section 6.5: Time step size k_m plotted over time t after 1 (left), 3 (middle) and 6 (right) adaptive refinements of the flapping test

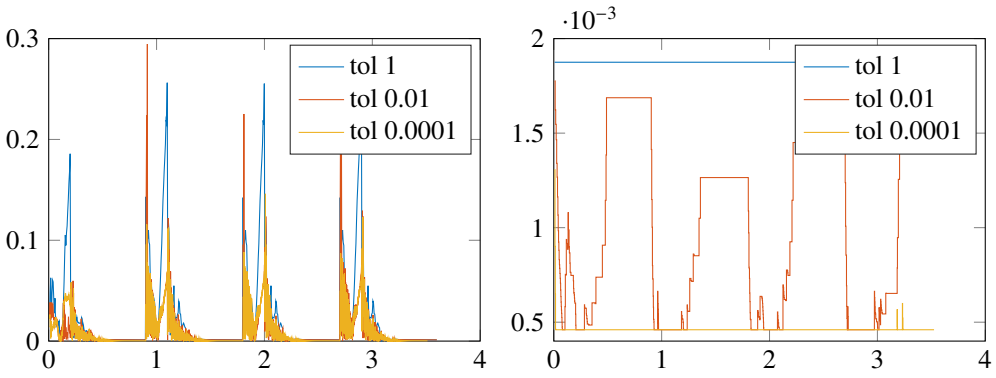

Figure 18: Section 6.5: Time step size k_m plotted over time t after heuristic time step refinements. At left, the absolute error $\eta_m = |j(U_{k,m}) - j(\tilde{U}_3)|$ is drawn. The smaller the chosen tolerance, the smaller the error in general. However, we observe from time to large error deflections, which happen at the largest flap deformation. At right, the time step sizes are plotted. For the largest tolerance, the upper bound $k_{max} = 1.875 \times 10^{-3} s$ of the time step size is taken, while for the smallest tolerance the lower time step size bound $k_{max} = 4.6 \times 10^{-4} s$ is adopted. In between, namely for the tolerance 0.01, the error estimator chooses small time step sizes when necessary, but then allow again for larger steps, when the numerical solution is smooth and the error in the goal functional is already sufficiently small.

7. Conclusion

In this work, we developed adaptive time step control for nonlinear variational-monolithic fluid-structure interaction. To realize the adaptive choice of time step sizes or intervals, we developed two methods. First, dual-weighted residual time error estimation in which an adjoint problem, running backward in time, needs to be solved. Secondly, we adopted an heuristic error estimator that is based on estimating the truncation error, a technique that is often used in other studies, but no detailed comparisons have been carried out yet for fluid-structure interaction. The developments of two error estimators in two different codes, allowed for one-by-one developments, that are not so often found in the literature. In the numerical examples, we made the following observations. First and most importantly, both codes yield the correct physical values proven by matching published benchmark results and comparing the numerical solutions to each other. Our findings for each numerical test can be summarized as follows: In the first example, we found that only the Fractional-Step-theta scheme works in a robust way. The Crank-Nicolson scheme lacks (as it is well-known) in robustness since it is only A-stable. The shifted Crank-Nicolson scheme works well, but depends on the correct choice of the shifting parameter. The Rannacher-scheme works well, too, but shows slight sub-oscillations in the drag value. In the Examples 2-4, we observed that adaptive time step control works in general well. For oscillating, but smooth inflow, adaptive time-stepping performs not that much better than uniform time step refinement. This is the case for the standard inflow profiles of the FSI benchmark tests. In order to strengthen these observations in more detail, we proposed modified non-smooth inflow profiles in which adaptive time step control pays off. In

these tests we also found that the heuristic estimator does also work, but it is hard to obtain quantitatively satisfying results with respect to the order of convergence. From these results, we infer that time step refinement based on the dual-weighted residual estimator is more reliable than heuristic time step refinement. This is obvious from a mathematical perspective, but now computationally demonstrated for fluid-structure interaction, i.e., a nonlinearly coupled multiphysics PDE system. While clearly both the development and implementation of the DWR estimator require more efforts than heuristic time step control, a second drawback of the latter one is the correct selection of certain model parameters. In ongoing future work, the goal is to combine temporal with spatial mesh adaptivity within optimal control problems. Here the adjoint problem can be used for both mesh adaptivity and the numerical solution of the optimization problem.

Acknowledgments

The first author gratefully acknowledges the support from the International Research Training Group IGDK 1754, funded by DFG and FWF, and from the International Graduate School of Science and Engineering at the Technische Universität München. Furthermore the first author gratefully acknowledges financial support by the Federal Ministry of Education and Research (BMBF) within the research grant "Modellierung, schnelle Simulation und Optimierung von Blutströmungen mit Materialschädigung". Moreover, we thank Thomas Richter and Dominik Meidner for providing their Navier-Stokes programming code developed in [50]. Finally, the first author is grateful for RICAM Linz' hospitality for the three-months research stay from May until July 2016. The second authors equally thanks his former institution for all the comfort to carry out half of the work of this paper.

Appendix

On the time discretized semi-linear forms

After applying the theta dependent quadrature rule and exploitation of the structure of the time discretized spaces, we obtain in the Problems 7 and 8 the following semi-linear forms:

$$
\begin{aligned}
\tilde{A}_F(U_{k,m}, U_{k,m-1})(\varphi_m) :=& \Big(\rho_f^0\Big[\theta_m J_{k,m} + (1-\theta_m) J_{k,m-1}\Big](v_{k,m} - v_{k,m-1}), \varphi_m\Big)_f \\
&- \Big[\theta_m \Big(\rho_f^0 J_{k,m} F_{k,m}^{-1}(u_{k,m} - u_{k,m-1}) \cdot \nabla v_{k,m}, \varphi_m\Big)_f \\
&\qquad + (1-\theta_m)\Big(\rho_f^0 J_{k,m-1} F_{k,m-1}^{-1}(u_{k,m} - u_{k,m-1}) \cdot \nabla v_{k,m-1}, \varphi_m\Big)_f \Big] \\
&+ k_m\Big[\theta_m \Big(\rho_f^0 J_{k,m}(F_{k,m}^{-1} v_{k,m} \cdot \nabla) v_{k,m}), \varphi_m\Big)_f \\
&\qquad + (1-\theta_m)\Big(\rho_f^0 J_{k,m-1}(F_{k,m-1}^{-1} v_{k,m-1} \cdot \nabla) v_{k,m-1}), \varphi_m\Big)_f \Big] \\
&+ k_m\Big[\theta_m \Big(J_{k,m}(\sigma_f)_{k,m} F_{k,m}^{-T}, \nabla\varphi_m\Big)_f \\
&\qquad + (1-\theta_m)\Big(J_{k,m-1}(\sigma_f)_{k,m-1} F_{k,m-1}^{-T}, \nabla\varphi_m\Big)_f \Big] \\
\tilde{A}_S(U_{k,m}, U_{k,m-1})(\varphi_m) :=& \Big(\rho_s^0(v_{k,m} - v_{k,m-1}), \varphi_m\Big)_s \\
&+ k_m\Big[\theta_m \Big(F_m(\Sigma_s)_{k,m}, \nabla\varphi_m\Big)_s + (1-\theta_m)\Big(F_{k,m-1}(\Sigma_s)_{k,m-1}, \nabla\varphi_m\Big)_s \Big]
\end{aligned}
$$

$$
\begin{aligned}
\tilde{A}_\Gamma(U_{k,m}, U_{k,m-1})(\varphi_m) :=& -\frac{k_m}{2}\Big[\theta_m\langle\rho_f^0\nu_f F_{k,m}^{-T}\nabla v_{k,m}^T, \varphi_m\rangle_{\Gamma^N} + (1-\theta_m)\langle\rho_f^0\nu_f F_{k,m-1}^{-T}\nabla v_{k,m-1}^T, \varphi_m\rangle_{\Gamma^N}\Big]\\
\tilde{A}_M(U_{k,m}, U_{k,m-1})(\psi) :=& k_m\Big[\theta_m\left((\sigma_m)_{k,m}, \nabla\psi_m\right)_f + (1-\theta_m)\left((\sigma_m)_{k,m-1}, \nabla\psi_m\right)_f\Big]\\
\tilde{A}_V(U_{k,m}, U_{k,m-1})(\psi) :=& \left(u_{k,m} - u_{k,m-1}, \psi_m\right)_s - k_m\Big[\left(\theta_m v_{k,m} + (1-\theta_m)v_{k,m-1}, \psi_m\right)_s\Big]\\
\tilde{A}_D(U_{k,m}, U_{k,m-1})(\xi) :=& \frac{k_m}{2}\left(\operatorname{div}(J_{k,m}F_{k,m}^{-1}v_{k,m}) + \operatorname{div}(J_{k,m-1}F_{k,m-1}^{-1}v_{k,m-1}), \xi\right)_f\\
\tilde{F}(U_{k,m}, U_{k,m-1})(\varphi) :=& k_m\Big[\theta_m\left(J_{k,m}\rho_f^0 f(t_m), \varphi_m\right)_f + (1-\theta_m)\left(J_{m-1}\rho_f^0 f(t_{m-1}), \varphi_m\right)_f\Big]\\
&+ k_m\Big[\theta_m\left(\rho_s^0 f(t_m), \varphi_m\right)_s + (1-\theta_m)\left(\rho_s^0 f(t_{m-1}), \varphi_m\right)_s\Big],
\end{aligned}
$$

and in addition the linear forms

$$
\tilde{I}_V(U_{k,0})(\varphi_0) := (v_0 - v_{k,0}, \varphi_0), \quad \tilde{I}_U(U_{k,0})(\psi_0) := (u_0 - u_{k,0}, \psi_0).
$$

Thereby, we denote with $J_{k,m}$, $F_{k,m}$, $(\sigma_f)_{k,m}$, $(\sigma_m)_{k,m}$ and $(\Sigma_s)_{k,m}$ the evaluation of the respective terms at the time point t_m^- and for the values with index $m-1$ the evaluation at t_{m-1}^+.

Derivatives of the bilinear form

In order to calculate sensitivities of the functional of interest we have to solve the adjoint equation. As already stated in Section 5, the adjoint equation includes the derivatives of the semi-linear form $A(U)(\Phi)$ with respect to the velocity variable v, the displacement u and the pressure p. For more details how to calculate the derivatives and the exact values of the derivatives of the stress tensors we refer to [67]. For the forms corresponding to the fluid equation we obtain

$$
\begin{aligned}
A'_{F,p}(U)(\xi, z^v) =& -\langle\!\langle J\frac{d\sigma_f}{dp}(\xi)F^{-T}, \nabla z^v\rangle\!\rangle_f\\
A'_{F,v}(U)(\varphi, z^v) =& \langle\!\langle\rho_f^0 J\partial_t\varphi, z^v\rangle\!\rangle_f + \langle\!\langle J\frac{d\sigma_f}{dv}(\varphi)F^{-T}, \nabla z^v\rangle\!\rangle_f\\
&+ \langle\!\langle\rho_f^0 J(F^{-1}\varphi\cdot\nabla)v), z^v\rangle\!\rangle_f + \langle\!\langle\rho_f^0 J(F^{-1}(v-\partial_t u)\cdot\nabla)\varphi), z^v\rangle\!\rangle_f\\
A'_{F,u}(U)(\psi, z^v) =& \langle\!\langle\rho_f^0 J\operatorname{tr}(F^{-1}\nabla\psi)\partial_t v, z^v\rangle\!\rangle_f - \langle\!\langle\rho_f^0 J(F^{-1}\partial_t\psi\cdot\nabla)v), z^v\rangle\!\rangle_f\\
&+ \langle\!\langle\rho_f^0 J\operatorname{tr}(F^{-1}\nabla\psi)(F^{-1}(v-\partial_t u)\cdot\nabla)v), z^v\rangle\!\rangle_f\\
&- \langle\!\langle\rho_f^0 J(F^{-1}\nabla\psi F^{-1}(v-\partial_t u)\cdot\nabla)v), z^v\rangle\!\rangle_f\\
&+ \langle\!\langle J\operatorname{tr}(F^{-1}\nabla\psi)\sigma_f F^{-T}, \nabla z^v\rangle\!\rangle_f - \langle\!\langle J\sigma_f F^{-T}\nabla\psi^T F^{-T}, \nabla z^v\rangle\!\rangle_f\\
&+ \langle\!\langle J\frac{d\sigma_f}{du}(\psi)F^{-T}, \nabla z^v\rangle\!\rangle_f.
\end{aligned}
$$

Thereby the derivatives of the fluid stress tensor is given by

$$
\begin{aligned}
\frac{d\sigma_f}{dp}(\xi) &= -\xi\,\mathrm{Id}\\
\frac{d\sigma_f}{dv}(\varphi) &= \rho_f\nu_f(\nabla\varphi F^{-1} + F^{-T}\nabla\varphi^T)\\
\frac{d\sigma_f}{du}(\psi) &= \rho_f\nu_f(-\nabla v_f F^{-1}\nabla\psi F^{-1} - F^{-T}\nabla\psi F^{-T}\nabla v_f^T).
\end{aligned}
$$

The linearization of the divergence condition results in

$$
\begin{aligned}
A'_{D,v}(U)(\varphi, z^p) =& \langle\!\langle\operatorname{div}(JF^{-1}\varphi), z^p\rangle\!\rangle_f\\
A'_{D,u}(U)(\psi, z^p) =& \langle\!\langle\operatorname{div}(J\operatorname{tr}(F^{-1}\nabla\psi)F^{-1}v), z^p\rangle\!\rangle_f - \langle\!\langle\operatorname{div}(JF^{-1}\nabla\psi F^{-1}v), z^p\rangle\!\rangle_f.
\end{aligned}
$$

If we calculate the derivatives of the nonlinear elastodynamic equations $A_S(U)(z^v)$ and $A_V(U)(z^u)$, we get

$$\begin{aligned}
A'_{S,v}(U)(\varphi, z^v) =& (\!(\rho_s^0 \partial_t \varphi, z^v)\!)_s \\
A'_{S,u}(U)(\psi, z^v) =& (\!(\nabla\psi \Sigma_s, \nabla z^v)\!)_s + (\!(F \frac{d\Sigma_s}{du}(\psi), \nabla z^v)\!)_s \\
A'_{V,v}(U)(\varphi, z^u) =& (\!(-\varphi, z^u)\!)_s \\
A'_{V,u}(U)(\psi, z^u) =& (\!(\psi_t, z^u)\!)_s.
\end{aligned}$$

Thereby the derivative of the solid stress tensor is given by

$$\begin{aligned}
\frac{d\Sigma_s}{du}(\psi) &= \lambda_s \operatorname{tr}(\frac{dE_s}{du}(\psi)) \operatorname{Id} + 2\mu_s \frac{dE_s}{du}(\psi) \\
\frac{dE_s}{du}(\psi) &= \frac{1}{2}(\nabla\psi^T F + F^T \nabla\psi).
\end{aligned}$$

On the outflow boundary we get due to the do-nothing outflow condition for the derivative of the term $A_\Gamma(U)(z^v)$:

$$\begin{aligned}
A'_{\Gamma,v}(U)(\varphi, z^v) =& - \langle\!\langle J \rho_f^0 \nu_f F^{-T} \nabla\varphi^T F^{-T} n_f, z^v \rangle\!\rangle_{\Gamma_{out}} \\
A'_{\Gamma,u}(U)(\psi, z^v) =& - \langle\!\langle J \operatorname{tr}(F^{-1}\nabla\psi) \rho_f^0 \nu_f F^{-T} \nabla v^T F^{-T} n_f, z^v \rangle\!\rangle_{\Gamma_{out}} \\
&+ \langle\!\langle J \rho_f^0 \nu_f F^{-T} \nabla\psi^T F^{-T} \nabla v^T F^{-T} n_f, z^v \rangle\!\rangle_{\Gamma_{out}} \\
&+ \langle\!\langle J \rho_f^0 \nu_f F^{-T} \nabla v^T F^{-T} \nabla\psi^T F^{-T} n_f, z^v \rangle\!\rangle_{\Gamma_{out}}.
\end{aligned}$$

The derivative of the mesh motion $A_M(U)(z^u)$ leads to

$$\begin{aligned}
A'_{M,u}(U)(\psi, z^u) &= (\!(\frac{d\sigma_m}{du}(\psi), \nabla z^u)\!)_f \\
&= (\!(\lambda_m \operatorname{tr}(\frac{1}{2}(\nabla\psi + \nabla\psi^T)) \operatorname{Id} + 2\mu_m \frac{1}{2}(\nabla\psi + \nabla\psi^T), \nabla z^u)\!)_f.
\end{aligned}$$

At first sight we would have to demand, that velocity and deformations are two times-differentiable to calculate the divergence. But according to [67] the divergence terms can be restated into:

$$\begin{aligned}
(\!(\operatorname{div}(JF^{-1}\varphi), z^p)\!)_f &= (\!(J \operatorname{tr}(\nabla\varphi F^{-1}), z^p)\!)_f \\
(\!(\operatorname{div}(Jtr(F^{-1}\nabla\psi)F^{-1}v), z^p)\!)_f &= (\!(J \operatorname{tr}(F^{-1}\nabla\psi) \operatorname{tr}(\nabla v F^{-1}), z^p)\!)_f \\
(\!(\operatorname{div}(JF^{-1}\nabla\psi F^{-1}v), z^p)\!)_f &= (\!(J \operatorname{tr}(\nabla v F^{-1}\nabla\psi F^{-1}), z^p)\!)_f.
\end{aligned}$$

Therefore, it is sufficient to use in our numerical calculations subspaces of H^1 Sobolev-spaces and furthermore the above equations help us to implement the adjoint equation.

References

[1] G. Avalos, I. Lasiecka, and R. Triggiani. Higher regularity of a coupled parabolic-hyperbolic fluid-structure interactive system. *Georgian Mathematical Journal*, 15(3):403–437, 2008.

[2] G. Avalos and R. Triggiani. The coupled PDE system arising in fluid/structure interaction. I. Explicit semigroup generator and its spectral properties. In *Fluids and waves*, volume 440 of *Contemp. Math.*, pages 15–54. Amer. Math. Soc., Providence, RI, 2007.

[3] W. Bangerth, D. Davydov, T. Heister, L. Heltai, G. Kanschat, M. Kronbichler, M. Maier, B. Turcksin, and D. Wells. The `deal.II` library, version 8.4. *Journal of Numerical Mathematics*, 24, 2016.

[4] W. Bangerth, R. Hartmann, and G. Kanschat. deal.II – a general purpose object oriented finite element library. *ACM Trans. Math. Softw.*, 33(4):24/1–24/27, 2007.

[5] Y. Bazilevs, K. Takizawa, and T. Tezduyar. *Computational Fluid-Structure Interaction: Methods and Applications*. Wiley, 2013.

[6] R. Becker and M. Braack. A finite element pressure gradient stabilization for the stokes equations based on local projections. *CALCOLO*, 38(4):173–199, December 2001.

[7] R. Becker and R. Rannacher. A feed-back approach to error control in finite element methods: basic analysis and examples. *East-West J. Numer. Math.*, 4:237–264, 1996.

[8] R. Becker and R. Rannacher. *An optimal control approach to error control and mesh adaptation in finite element methods*, pages 1–102. Acta Numerica 2001, Cambridge University Press, a. iserles edition, 2001.
[9] M. Besier and R. Rannacher. Goal-oriented apace-time adaptivity in the finite element galerkin method for the computation of nonstationary incomressible flow. *International Journal for Numerical Methods in Fluids*, 70:1139–1166, 2012.
[10] P. Birken, K. J. Quint, S. Hartmann, and A. Meister. A time-adaptive fluid-structure interaction method for thermal coupling. *Computing and Visualization in Science*, 13(7):331–340, 2010.
[11] S. C. Brenner and L. R. Scott. *The mathematical theory of finite element methods*, volume 15 of *Texts in Applied Mathematics*. Springer-Verlag, New York, 1994.
[12] M. Bristeau, R. Glowinski, and J. Periaux. Numerical methods for the Navier-Stokes equations. *Comput. Phys. Rep.*, 6:73–187, 1987.
[13] H.-J. Bungartz, M. Mehl, and M. Schäfer, editors. *Fluid Structure Interaction II: Modelling, Simulation, Optimization*. Springer, Berlin, 2010.
[14] H.-J. Bungartz and M. Schäfer. *Fluid-Structure Interaction: Modelling, Simulation, Optimization*, volume 53 of *Lecture Notes in Computational Science and Engineering*. Springer, 2006.
[15] P. Causin, J.-F. Gerbeau, and F. Nobile. Added-mass effect in the design of partitioned algorithms for fluid-structure problems. *Comput. Methods Appl. Mech. Engrg.*, 194:4506–4527, 2005.
[16] P. G. Ciarlet. *The finite element method for elliptic problems*. North-Holland Publishing Co., Amsterdam-New York-Oxford, 1978. Studies in Mathematics and its Applications, Vol. 4.
[17] D. Coutand and S. Shkoller. Motion of an elastic solid inside an incompressible viscous fluid. *Arch. Rational Mech. Anal.*, 176:25–102, 2005.
[18] D. Coutand and S. Shkoller. The interaction between quasilinear elastodynamics and the Navier-Stokes equations. *Arch. Rational Mech. Anal.*, 179:303–352, 2006.
[19] T. A. Davis and I. S. Duff. An unsymmetric-pattern multifrontal method for sparse LU factorization. *SIAM J. Matrix Anal. Appl.*, 18(1):140–158, 1997.
[20] J. Donéa, P. Fasoli-Stella, and S. Giuliani. Lagrangian and Eulerian finite element techniques for transient fluid-structure interaction problems. In *Trans. 4th Int. Conf. on Structural Mechanics in Reactor Technology*, page Paper B1/2, 1977.
[21] Q. Du, M. D. Gunzburger, L. Hou, and J. Lee. Analysis of a linear fluid-structure interaction problem. *Disc. Cont. Dyn. Syst.*, 9(3):633–650, 2003.
[22] Q. Du, M. D. Gunzburger, L. Hou, and J. Lee. Semidiscrete finite element approximation of a linear fluid-structure interaction problem. *SIAM J. Numer. Anal*, 42(1):1–29, 2004.
[23] T. Dunne. An Eulerian approach to fluid-structure interaction and goal-oriented mesh adaption. *Int. J. Numer. Methods in Fluids*, 51:1017–1039, 2006.
[24] T. Dunne, R. Rannacher, and T. Richter. Numerical simulation of fluid-structure interaction based on monolithic variational formulations. In *Comtemporary Challenges in Mathematical Fluid Mechanics*. World Scientific, 2009.
[25] L. Failer. *Optimal control of time-dependet nonlinear fluid-structure interaction*. PhD thesis, Technische Universität München, 2017.
[26] P. Fick, E. Brummelen, and K. Zee. On the adjoint-consistent formulation of interface conditions in goal-oriented error estimation and adaptivity for fluid-structure interaction. *Computer Methods in Applied Mechanics and Engineering*, 199:3369–3385, 2010.
[27] L. Formaggia and F. Nobile. A stability analysis for the arbitrary Lagrangian Eulerian formulation with finite elements. *East-West Journal of Numerical Mathematics*, 7:105 – 132, 1999.
[28] L. Formaggia, A. Quarteroni, and A. Veneziani. *Cardiovascular Mathematics: Modeling and simulation of the circulatory system*. Springer-Verlag, Italia, Milano, 2009.
[29] S. Frei, T. Richter, and T. Wick. Long-term simulation of large deformation, mechano-chemical fluid-structure interactions in {ALE} and fully eulerian coordinates. *Journal of Computational Physics*, 321:874 – 891, 2016.
[30] G. Galdi and R. Rannacher. *Fundamental Trends in Fluid-Structure Interaction*. World Scientific, 2010.
[31] A. J. Gil, A. A. Carreno, J. Bonet, and O. Hassan. The immersed structural potential method for haemodynamic applications. *J. Comp. Physics*, 229:8613–8641, 2010.
[32] C. Goll, R. Rannacher, and W. Wollner. The damped Crank-Nicolson time-marching scheme for the adaptive solution of the Black-Scholes equation. *J. Comput. Finance*, 18(4):1–37, 2015.
[33] C. Grandemont. Existence of weak solutions for the unsteady interaction of a viscous fluid with an elastic plate. *SIAM J. Math. Anal.*, 40(2):716–737, 2008.
[34] T. Grätsch and K.-J. Bathe. Goal-oriented error estimation in the analysis of fluid flows with structural interactions. *Comp. Methods Appl. Mech. Engrg.*, 195:5673–5684, 2006.
[35] K. Gustafsson, M. Lundh, and G. Soederlind. A PI stepsize control for the numerical solution of ordinary differential equations. *BIT*, 28(2):270–287, 1988.
[36] A. Hay, S. Etienne, D. Pelletier, and A. Garon. hp-adaptive time integration based on the bdf for viscous flows. *Journal of Computational Physics*, 291:151 – 176, 2015.
[37] J. G. Heywood and R. Rannacher. Finite-element approximation of the nonstationary Navier-Stokes problem part iv: Error analysis for second-order time discretization. *SIAM Journal on Numerical Analysis*, 27(2):353–384, 1990.
[38] J. G. Heywood, R. Rannacher, and S. Turek. Artificial boundaries and flux and pressure conditions for the incompressible Navier-Stokes equations. *International Journal of Numerical Methods in Fluids*, 22:325–352, 1996.
[39] C. Hirt, A. Amsden, and J. Cook. An arbitrary Lagrangian-Eulerian computing method for all flow speeds. *J. Comput. Phys.*, 14:227–253, 1974.
[40] J. Hron and S. Turek. *A monolithic FEM/Multigrid solver for ALE formulation of fluid structure with application in biomechanics*, volume 53, pages 146–170. Springer-Verlag, 2006.
[41] J. Hron and S. Turek. *Proposal for numerical benchmarking of fluid-structure interaction between an elastic object and laminar incompressible flow*, volume 53, pages 146 – 170. Springer-Verlag, 2006.
[42] T. Hughes, W. Liu, and T. Zimmermann. Lagrangian-Eulerian finite element formulation for incompressible viscous flows. *Comput. Methods*

Appl. Mech. Engrg., 29:329–349, 1981.
[43] M. Ignatova, I. Kukavica, I. Lasiecka, and A. Tuffaha. On well-posedness for a free boundary fluid-structure model. *J. Math. Phys.*, 53(11):115624, November 2012.
[44] V. John and J. Rang. Adaptive time step control for the incompressible navierstokes equations. *Computer Methods in Applied Mechanics and Engineering*, 199(912):514 – 524, 2010.
[45] D. A. Kay, P. M. Gresho, D. F. Griffiths, and D. J. Silvester. Adaptive time-stepping for incompressible flow part ii: Navierstokes equations. *SIAM Journal on Scientific Computing*, 32(1):111–128, 2010.
[46] K. Kunsich and B. Vexler. Optimal vortex reduction for instationary flows based on translation invariant cost functionals. *SIAM J. Control Optim.*, 46(4):1368–1397, 2007.
[47] M. Luskin and R. Rannacher. On the soothing property of the Crank-Nicolson scheme. *Applicable Analysis*, 14(2):117 – 135, 1980.
[48] M. Mayr, T. Kloeppel, W. Wall, and M. Gee. A temportal consistent monolithic approach to fluid-structure interaction enabling single field predictors. *SIAM J. Sci. Comput.*, 37(1):B30–B59, 2015.
[49] D. Meidner and T. Richter. Goal-oriented error estimation for the fractional step theta scheme. *Comput. Methods Appl. Math.*, 14(2):203–230, 2014.
[50] D. Meidner and T. Richter. A posteriori error estimation for the fractional step theta discretization of the incompressible Navier-Stokes equations. *Comput. Methods Appl. Mech. Engrg.*, 288:45–59, 2015.
[51] W. Noh. *A time-dependent two-space-dimensional coupled Eulerian-Lagrangian code*, volume 3 of *Methods Comput. Phys.*, pages 117–179. Academic Press, New York, 1964.
[52] A. Okubo. Horizontal dispersion of floatable particles in the vicinity of velocity singularities such as convergences. *Deep Sea Research and Oceanographic Abstracts*, 17(3):445 – 454, 1970.
[53] R. Rannacher. Finite element solution of diffusion problems with irregular data. *Numer. Math.*, 43:309–327, 1984.
[54] R. Rannacher. On the stabilization of the Crank-Nicolson scheme for long time calculations. Preprint, August 1986.
[55] T. Richter. *Parallel Multigrid Method for Adaptive Finite Elements with Application to 3D Flow Problems*. PhD thesis, University of Heidelberg, 2005.
[56] T. Richter. Goal-oriented error estimation for fluid-structure interaction problems. *Comput. Methods Appl. Mech. Engrg.*, pages 28–42, 2012.
[57] T. Richter. Lecture on fluid-structure interaction. WS2012. will appear as Springer book in October 2017, http://www.springer.com/de/book/9783319639697.
[58] T. Richter and T. Wick. Finite elements for fluid-structure interaction in ALE and fully Eulerian coordinates. *Comput. Methods Appl. Mech. Engrg.*, 199:2633–2642, 2010.
[59] T. Richter and T. Wick. On time discretizations of fluid-structure interactions. In T. Carraro, M. Geiger, S. Körkel, and R. Rannacher, editors, *Multiple Shooting and Time Domain Decomposition Methods*, pages 377–400, Contributions in Mathematical and Computational Science, 2015.
[60] RoDoBo. A C++ library for optimization with stationary and nonstationary PDEs.
[61] M. Schäfer and S. Turek. *Flow Simulation with High-Performance Computer II*, volume 52 of *Notes on Numerical Fluid Mechanics*, chapter Benchmark Computations of laminar flow around a cylinder. Vieweg, Braunschweig Wiesbaden, 1996.
[62] M. Schmich and B. Vexler. Adaptivity with dynamic meshes for space-time finite element discretizations of parabolic equations. *SIAM J. Sci. Comput.*, 30(1):369–393, 2007/08.
[63] T. Tezduyar, M. Behr, and J. Liou. A new strategy for finite element computations involving moving boundaries and interfaces - the deforming-spatial-domain/space-time procedure: I. the concept and the preliminary numerical tests. *Comp. Methods Appl. Mech. Engrg.*, 94:339–351, 1992.
[64] T. Tezduyar, M. Behr, S. Mittal, and J. Liou. A new strategy for finite element computations involving moving boundaries and interfaces - the deforming-spatial-domain/space-time procedure: II. Computation of free-surface flows, two-liquid flows, and flows with drifting cylinders. *Comp. Methods Appl. Mech. Engrg.*, 94:353–371, 1992.
[65] S. Turek. *Efficient solvers for incompressible flow problems*. Springer-Verlag, 1999.
[66] J. Weiss. The dynamics of enstrophy transfer in two-dimensional hydrodynamics. *Phys. D*, 48(2-3):273–294, 1991.
[67] T. Wick. *Adaptive Finite Element Simulation of Fluid-Structure Interaction with Application to Heart-Valve Dynamics*. PhD thesis, University of Heidelberg, 2011.
[68] T. Wick. Fluid-structure interactions using different mesh motion techniques. *Computers and Structures*, 89(13-14):1456–1467, 2011.
[69] T. Wick. Goal-oriented mesh adaptivity for fluid-structure interaction with application to heart-valve settings. *Arch. Mech. Engrg.*, 59(6):73–99, 2012.
[70] T. Wick. Solving monolithic fluid-structure interaction problems in arbitrary Lagrangian Eulerian coordinates with the deal.II library. *Archive of Numerical Software*, 1:1–19, 2013.
[71] T. Wick. Flapping and contact FSI computations with the fluid-solid interface-tracking/interface-capturing technique and mesh adaptivity. *Computational Mechanics*, 53(1):29–43, 2014.
[72] K. Zee, E. Brummelen, I. Akkerman, and R. Borst. Goal-oriented error estimation and adaptivity for fluid-structure interaction using exact linearized adjoints. *CMAME*, 200:2738–2757, 2011.